# Disentangling neuronal inhibition and inhibitory pathways in the lateral habenula

Jack F. Webster[1], Rozan Vroman[1], Shuzo Sakata[1] and Christian Wozny[1,*]

[1] Strathclyde Institute of Pharmacy and Biomedical Sciences
University of Strathclyde
161 Cathedral Street
Glasgow
G4 0RE, UK

* Corresponding author: christian.wozny@strath.ac.uk
Phone: +44 (0)141 548 2122

## Abstract

The lateral habenula (LHb) is hyperactive in depression, and thus inhibition of this structure makes an interesting target for future antidepressant therapies. However, the circuit mechanisms mediating inhibitory signalling within the LHb are not well-known. We addressed this issue by studying LHb neurons expressing either parvalbumin (PV) or Neuron-derived neurotrophic factor (Ndnf), two markers of particular sub-classes of neocortical inhibitory neurons. In the LHb, we report that Ndnf is not representative of any particular neuronal sub-population. In contrast, we find that PV is expressed by multiple physiologically diverse sub-classes of LHb neurons. Furthermore, we identify two previously unknown distinct sources of inhibitory input arising from PV-positive neurons both locally, and from the medial dorsal thalamic nucleus. These findings hence provide new insight into inhibitory control within the LHb, and highlight that this structure is more neuronally diverse than previously thought.

## Acknowledgement

We are grateful to Hongkui Zeng from the Allen Brain Institute, Seattle, for kindly sharing the Ai9 reporter mice with us, and we thank Csaba Földy, Brain Research Institute, University of Zurich, Switzerland, for generously providing us with NPY-hrGFP mice.

This work was supported by a Royal Society Research Grant, RG160549 (C.W.), a Wellcome Trust Seed Award, 205917/z/17/Z (C.W.), Small Research Grant from Tenovus Scotland, Project S16/19 (C.W.), and BBSRC (BB/M00905X/1 to S.S.).

J.F.W. holds a studentship funded by the Engineering and Physical Sciences Research Council (EPSRC).

We further thank the Wozny lab for helpful discussions. The authors have no financial conflicts of interest.

## Contributions

J.F.W. performed the experiments. R.V. contributed to experiments. J.F.W. analysed the data. C.W. designed and supervised the study and helped J.F.W writing the manuscript. R.V. and S.S. contributed to the manuscript and discussions.

## Introduction

The lateral habenula (LHb) is an epithalamic brain structure, which acts as an inhibitory modulator of the midbrain reward circuitry, including the ventral tegmental area (VTA)[1–3] and the raphe nuclei[4]. Recently, the LHb has drawn renewed attention[5] due to the revelation that it becomes pathologically hyperactive in major depressive disorder (MDD)[6–12], thus providing excessive inhibition to these reward centres and silencing the associated positive emotions. Concurrently, this makes the LHb an intriguing target for novel antidepressant therapies[6,7,9,11–14]. Notably, multiple studies have shown that potentiation of inhibition within the LHb yields an antidepressant effect[9,10,13,15], likely by disinhibition of the reward circuitry. Despite this, however, the neural circuitry which mediates inhibitory signalling within the LHb is not well understood. To date, very few populations of local inhibitory neurons have been identified within the LHb[16–18], and external inhibitory input appears to arise primarily from GABA / glutamate co-releasing fibres[8,19–21]. Yet the LHb does receive a large inhibitory input[9,17], and recently some exclusively GABAergic fibres have been reported to project to it[15,22,23]. It is hence likely that other as-of-yet undefined circuitry components mediate inhibitory signalling within the LHb, and studying these may yield further insights into the underlying mechanisms by which it is implicated in the pathogenesis of MDD.

We therefore sought to address this issue of inhibitory control within the LHb. Parvalbumin (PV) has long been accepted as a neuronal marker associated with particular sub-populations of inhibitory interneurons within many structures throughout the brain including the neocortex[24], hippocampus[25] and striatum[26]. Neurogliaform cells, or at least neurons with almost identical characteristics to those in the neocortex,

have reportedly been identified within the LHb[16,17], however their function remains elusive. Neuron-derived neurotrophic factor (Ndnf) has recently been proposed to be expressed selectively by neocortical neurogliaform cells[27–29], while neuropeptide Y (NPY) is also an accepted, although not entirely selective, marker of these neurons[30].

Referring to the question of inhibitory control within the LHb, we therefore asked if these markers also represented distinct sub-populations of inhibitory neurons within this structure, and aimed to characterise the circuitry formed by neurons expressing them. In contrast to other brain regions, we find that Ndnf and NPY are not confined to any particular sub-population of LHb neuron. Strikingly, however, we report distinct sources of inhibitory input to the LHb from PV-positive neurons, arising from both locally-targeting LHb neurons, and from neurons in the medial dorsal thalamic nucleus.

## Results

### Excitatory and inhibitory transmission within the lateral habenula

GABAergic signalling has previously been reported in the LHb[9,20]. To assess the balance of excitation and inhibition within the LHb, we simultaneously recorded spontaneous excitatory and inhibitory currents in LHb neurons using a low chloride intracellular recording solution (Fig. 1a; n = 10 neurons; N = 5 mice). For comparison, we recorded spontaneous events in L2/3 pyramidal neurons in the somatosensory cortex (n = 9; N = 4 mice). While the ratio of excitatory to inhibitory events was far larger in LHb neurons than in cortical neurons (Fig. 1b; 22.9 vs 2.3, respectively), we could clearly observe inhibitory currents with comparable frequency (Fig. 1c; 0.1 ± 0.0

Hz vs 0.5 ± 0.3 Hz, respectively; $p$ = 0.23; two-tailed unpaired t-test), amplitude (Fig. 1c; 13.8 ± 1.3 pA vs 12.6 ± 1.1 pA, respectively; $p$ = 0.49; two-tailed unpaired t-test) and kinetics (Fig. 1d; rise time 1.3 ± 0.2 ms vs 1.0 ± 0.1 ms, respectively; $p$ = 0.11; half-width 2.1 ± 0.3 ms vs 1.7 ± 0.4 ms, respectively; $p$ = 0.45; decay 16.1 ± 3.4 ms vs 13.4 ± 4.1 ms, respectively; $p$ = 0.64; two-tailed unpaired t-test) to those in cortical neurons. Hence we asked whether these events could be mediated by similar inhibitory neurons as those in the cortex.

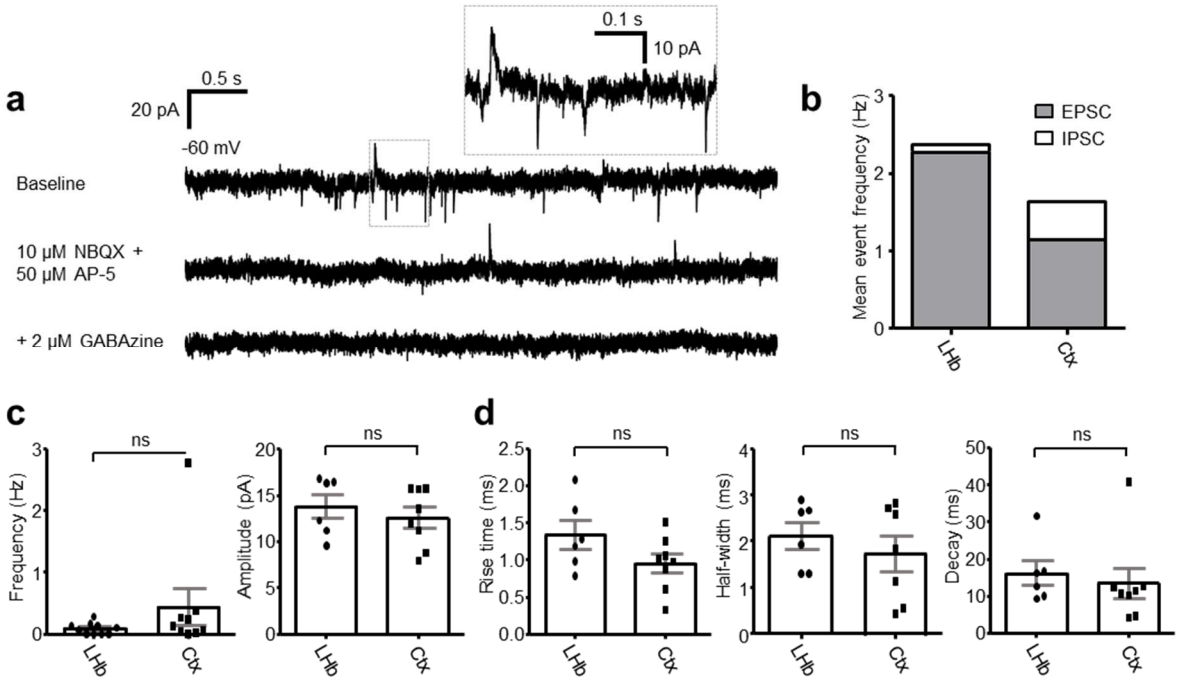


**Figure 1: Spontaneous inhibitory currents within the lateral habenula and somatosensory cortex. (a)** Example traces of spontaneous currents in an LHb neuron recorded in voltage clamp configuration. AMPA and NMDA-mediated excitatory currents and $GABA_A$-mediated inward currents could be observed simultaneously using a low-chloride intracellular solution. **(b)** Relative frequency of excitatory vs inhibitory currents in both LHb neurons (n = 10 neurons from 5 mice) and

113 somatosensory cortex L2/3 pyramidal neurons (n = 9 neurons from 4 mice). **(c)**
114 Comparison of frequency (left) and amplitude (right) between inhibitory currents in LHb
115 neurons and L2/3 pyramidal neurons. Data are mean ± SEM. **(d)** Comparison of
116 kinetics (rise time, half-width and decay) between inhibitory currents in LHb neurons
117 and L2/3 pyramidal neurons. Note for 4 LHb neurons, and 1 cortical neuron, no
118 inhibitory currents were observed. For these neurons, frequency value was 0 Hz.
119 However, as there were no measurable currents, these neurons have been excluded
120 from analyses of current amplitude and kinetics.

121

122 **Ndnf and NPY do not act as selective markers for inhibitory neurons within the**
123 **LHb**

124 Similar to reports in the neocortex[27–30], we first asked if Ndnf or NPY could act as
125 selective markers for particular sub-populations of inhibitory neurons within the LHb.
126 To test this we first made use of NPY-hrGFP mice, where GFP is expressed in NPY-
127 positive neurons. Brains from these mice (N = 2) were sectioned in the coronal plane
128 and imaged on a confocal microscope. In slices from NPY-hrGFP mice, while we did
129 observe some sparse fibres in the LHb, we did not observe any NPY-positive somata
130 (Fig. S1). We next crossed Ndnf-IRES-Cre mice to Ai9 reporter mice, so as to generate
131 Ndnf-IRES-Cre::Ai9 offspring (N = 2), which expressed TdTomato in Ndnf-positive
132 neurons (Fig. 2a). We did observe Ndnf-positive somata within the LHb in slices from
133 Ndnf-IRES-Cre::Ai9 mice. However, only a small sub-population of these (14.3 %) co-
134 localised with GABA (Fig. 2b and c). For comparison, we also imaged Ndnf expression
135 in the somatosensory cortex. While Ndnf expression was largely confined to
136 neocortical layer 1 (L1) in these slices, we also observed some expression in deeper

137 cortical layers (Fig. S2a). Additionally, most (75.8 %) but not all Ndnf-positive somata
138 co-localised with GABA (Fig. S2b), consistent with recent reports that Ndnf expression
139 is not entirely confined to L1 neurogliaform cells in the neocortex[28,29].

140 To gain a better insight into the characteristics of Ndnf-positive LHb neurons, we
141 also characterised their physiological properties in acute slices from Ndnf-IRES-
142 Cre::Ai9 mice (n = 29; N = 5 mice). In two of these cells, action potential discharge
143 could not be elicited upon current injection and hence we assumed these to be glial
144 cells and excluded from further analysis. We assessed passive physiological
145 properties in the remainder (n = 27) and observed no difference in resting membrane
146 potential in comparison to recordings from the general population of neurons in wild-
147 type C57/BL6 mice (Fig. 2d; n = 28 from 5 mice; -54.6 ± 1.3 vs -55.2 ± 1.4; $p$ = 0.78;
148 two-tailed unpaired t-test). We did, however, observe a significant difference in input
149 resistance (Fig. 2d; 775.9 ± 76.5 vs 544.0 ± 53.3; $p$ = 0.03; two-tailed unpaired t-test).
150 This was likely due to the fact that many recorded Ndnf-positive neurons were located
151 on the boundary with the medial habenula (Fig. 2e; n = 9), where neurons are known
152 to have very high input resistances[31]. This finding also supports the notion of the
153 recently identified intermediary region between the lateral and medial habenula
154 consisting of intermingled neurons from both regions[32]. Otherwise, physiological
155 properties of Ndnf-positive LHb neurons were largely consistent with previously
156 described LHb neuronal physiologies[16,33,34] in that almost all (n = 22 from 24 neurons
157 tested) displayed rebound action potential discharge upon hyperpolarizing current
158 injection, and a combination of tonic and bursting action potential discharge upon
159 depolarizing current injection (Fig. 2fi). We also reconstructed a small subset of these
160 neurons (n = 5) and observed that all neurons reconstructed exhibited 4-6 primary

161 dendrites, and a long unbranching axon (Fig. 2fii), therefore lacking the characteristic
162 axonal arbour that is a hallmark of neocortical neurogliaform cells[30].

163 To examine whether Ndnf-positive axonal fibres can elicit inhibitory transmission in
164 the LHb, we next crossed Ndnf-IRES-Cre mice to Ai32[35] reporter mice, to generate
165 offspring that express ChR2 and eYFP in Ndnf-positive neurons (Fig. 2g). We created
166 acute slices from these mice (N = 6) and recorded postsynaptic potentials in LHb
167 neurons (Fig. 2h; n = 21) in response to photostimulation. In the LHb, most responsive
168 neurons (n = 5 of 6) displayed a solely excitatory postsynaptic potential (EPSP), while
169 one neuron displayed a postsynaptic potential with both an NBQX-sensitive excitatory
170 component and a GABAzine-sensitive inhibitory component (Fig. 2i and j). These
171 responses were spread fairly evenly throughout the LHb (Fig. 2k), consistent with
172 confocal imaging of serial coronal sections from Ndnf-IRES-Cre::Ai32 mice (N = 2), in
173 that both Ndnf-positive fibres and somata were dispersed evenly throughout the LHb
174 (Fig. S3).

175 As a control, we also recorded photostimulation-induced postsynaptic potentials in
176 L2/3 pyramidal neurons (Fig. S2c) in acute slices from Ndnf-IRES-Cre::Ai32 (Fig. S2d-
177 f; n = 7; N = 6). Neurogliaform cells are known to mediate slow inhibition, with IPSPs
178 mediated by these neurons having larger $GABA_B$-components than other interneuron
179 sub-classes[36–39]. Therefore, we also expressed ChR2 in PV-positive neurons (termed
180 PV-IRES-Cre::Ai32 mice) and compared L2/3 pyramidal neuron IPSPs in Ndnf-IRES-
181 Cre::Ai32 slices to those in PV-IRES-Cre::Ai32 slices (Fig. S2d; n = 7; N = 6) upon
182 photostimulation. Consistently, we observed large IPSPs with comparable amplitude
183 in both lines, but with slower kinetics in the Ndnf-IRES-Cre::Ai32 slices (Fig. S2d)
184 indicative of a large $GABA_B$-component. Interestingly, in two neurons from Ndnf-IRES-

185 Cre::Ai32 slices, $GABA_A$ and $GABA_B$-blockade unmasked a small AMPA-mediated
186 excitatory component (Fig. S2e and f). As with the Ndnf-IRES-Cre::Ai9 line, post-hoc
187 confocal imaging of these slices also revealed some Ndnf-positive somata outside of
188 L1 (Fig. S2g), hence confirming findings from recent reports[27–29] that Ndnf is largely,
189 but not exclusively, confined to neocortical L1 inhibitory neurons.

190 Together, these results hence suggest that neither NPY nor Ndnf are selectively
191 expressed by locally-targeting inhibitory neurons within the LHb. Instead, we find that
192 no LHb neurons are NPY-positive, and that Ndnf is not expressed selectively by any
193 sub-class of LHb neuron.

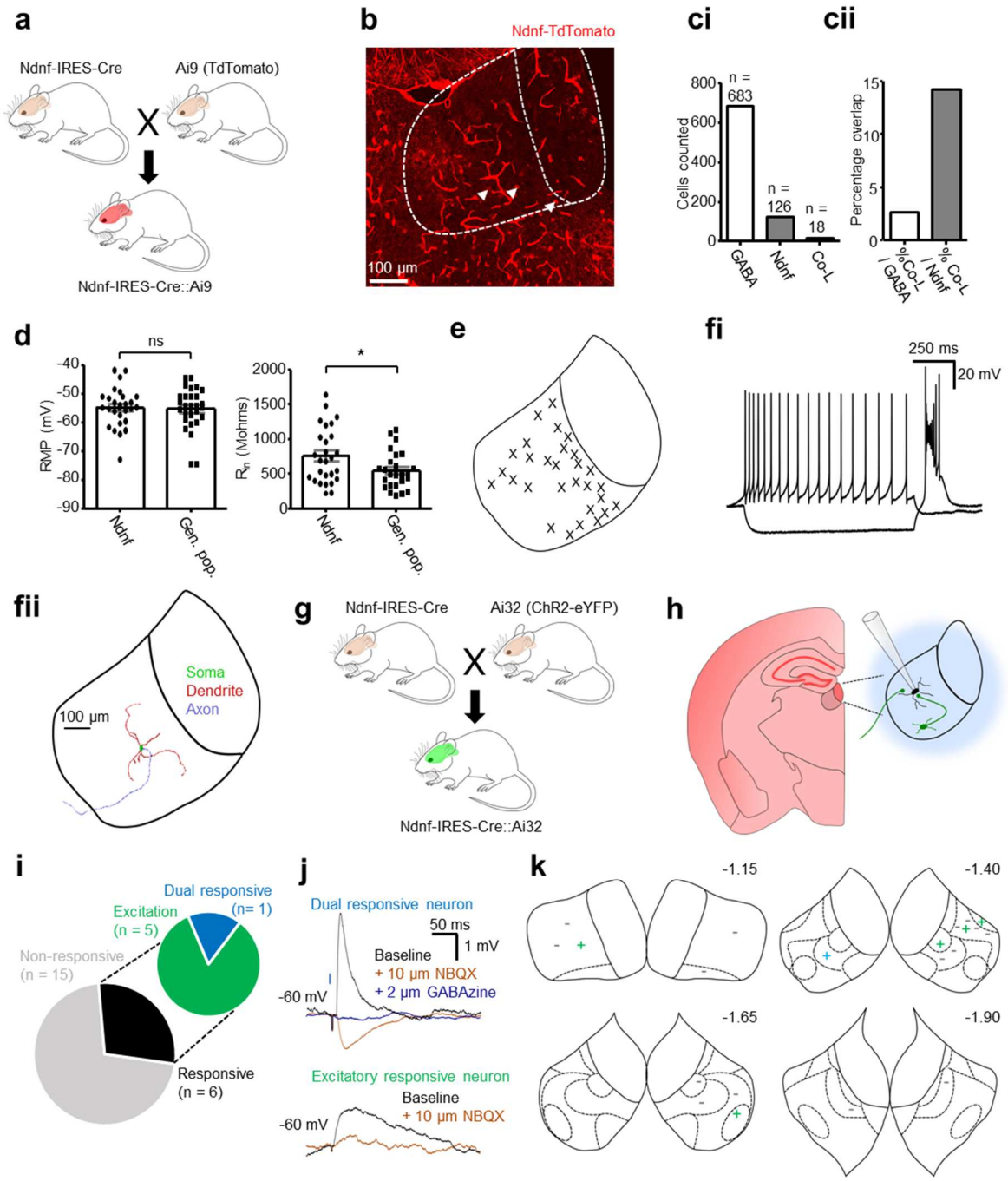


**Figure 2: Ndnf neurons are primarily non-inhibitory within the LHb. (a)** Schematic illustrating breeding scheme for generating Ndnf-IRES-Cre::Ai9 mice. **(b)** Confocal micrograph from an Ndnf-IRES-Cre::Ai9 mouse depicting Ndnf-positive neurons within the LHb (arrowheads). **(ci)** Bar chart quantifying total number of GABA-immunoreactive, and Ndnf-positive neurons counted and the number which co-expressed both (N = 2 mice). **(cii)** Fraction of neurons expressing both markers as a

201 percentage of GABA-immunoreactive neurons, and as a percentage of Ndnf-positive
202 neurons. **(d)** Comparison of passive properties of Ndnf-positive LHb neurons (n = 27;
203 N = 5 mice) and from the general population of LHb neurons recorded in C57 mice (n
204 = 28; N = 5 mice). Data are mean ± SEM. **(e)** Schematic illustrating location of patched
205 neurons throughout the habenular complex. In this case, all neurons recorded have
206 been compressed onto one schematic to allow clear visualization of neurons recorded
207 near the border with the medial habenula vs throughout the rest of the LHb. **(fi)**
208 Example traces from an Ndnf-positive neuron in response to current injection. Current
209 steps: -50 pA and 50 pA; 1 s duration. (**fii**) Example morphological reconstruction from
210 an Ndnf-positive neuron. All reconstructed neurons (n = 5) displayed 4-6 primary
211 dendrites and a single unbranching axon. **(g)** Schematic illustrating breeding scheme
212 for generating Ndnf-IRES-Cre::Ai32 mice. **(h)** Schematic of recording scheme. LHb
213 neurons were patched and blue light was used to stimulate both local and long-
214 distance Ndnf-positive neurons. **(i)** Pie chart quantifying fraction of neurons responsive
215 to photostimulation, and the nature of those responses. **(j)** Example traces from two
216 separate neurons in which photostimulation elicited a response with both an NBQX-
217 sensitive excitatory component, and a GABAzine-sensitive inhibitory component (top)
218 and from a neuron in which photostimulation elicited an excitatory response (bottom).
219 **(k)** Schematic illustrating location of patched neurons within the habenular complex,
220 projected rostrally (top left) through caudally (bottom right). Non-responsive neurons
221 are indicated by – while responsive neurons are indicated by: + EPSP only; + dual
222 response. Sub-nuclear boundaries as defined by Andres et al., (1999) are indicated
223 by dashed lines. Approximate rostral-caudal distances from Bregma (in mm) are
224 indicated.

225 **PV-positive lateral habenular neurons form multiple physiologically distinct**
226 **sub-classes**

227 PV-positive neurons are a well-defined sub-class of locally-targeting inhibitory neurons
228 in several major brain structures such as the neocortex[24] and hippocampus[25].
229 Considering that we observed inhibitory currents in the LHb comparable to those in
230 the neocortex (Fig. 1), we therefore asked if PV-positive neurons could be mediating
231 inhibition within the LHb.

232 To address this question, we first implemented a histological approach and asked
233 if PV-positive neurons in the LHb are GABAergic (Figs. 3 & S4). Within the LHb,
234 neurons co-labelled with PV and GABA antibodies were clearly visible and appeared
235 to be confined to the lateral portion of the LHb (Fig. 3a and b). However, these only
236 represented a small sub-population (8.8 %; N = 3 mice) of total PV-positive LHb
237 neurons (Fig. 3c). The remainder were non-GABAergic (Fig. 3a and c) and appeared
238 to be mostly localized within two distinct clusters; one within the medial LHb and one
239 within the lateral LHb along the rostral-caudal axis (Fig. 3b). As a control, we also
240 quantified co-labelling in the somatosensory cortex where all PV-positive neurons are
241 known to be inhibitory[24]. Within layers 2/3 of the somatosensory cortex, nearly all (98.1
242 %; N = 3 mice) PV-immunoreactive neurons were also GABA-immunoreactive (Fig.
243 S4). While these results do indicate the existence of a small sub-population of
244 GABAergic PV-positive LHb neurons, we find that the majority of PV-positive LHb
245 neurons are not GABAergic.

246

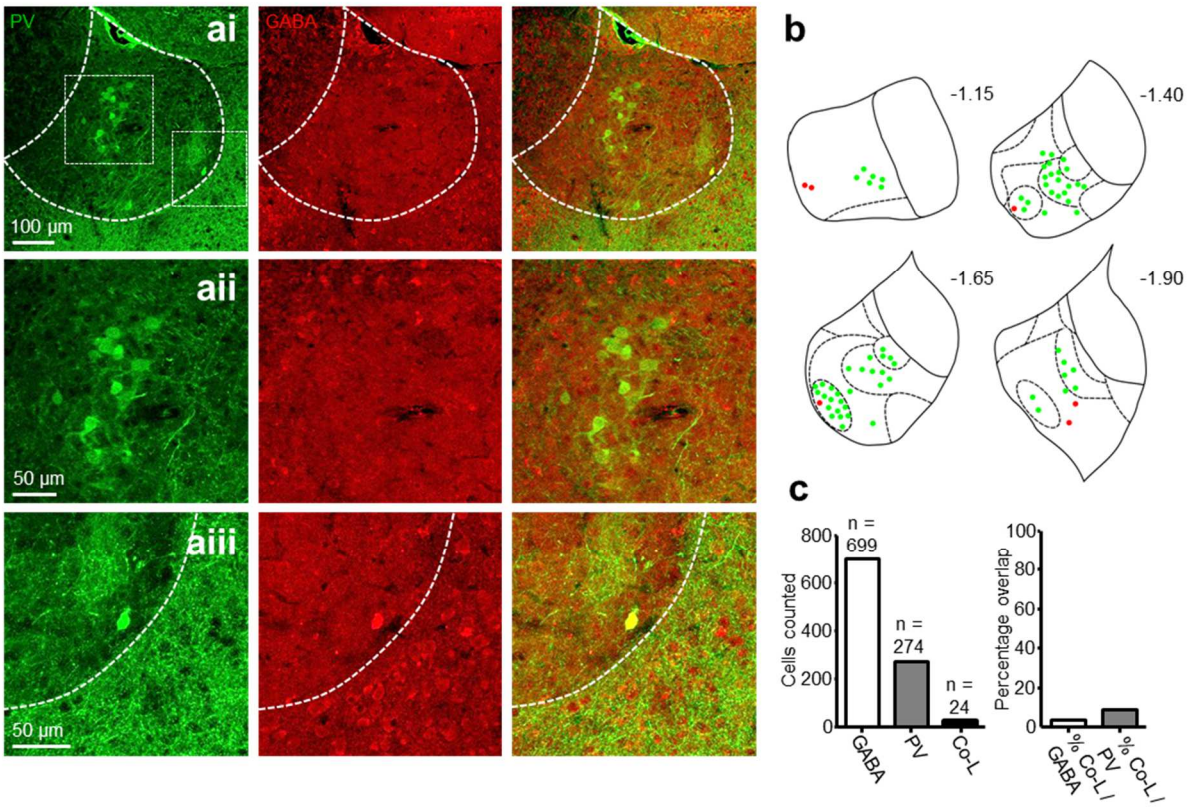


247

248 **Figure 3: PV-immunoreactive neurons within the lateral habenula are primarily**
249 **non-GABAergic. (ai)** 20x representative confocal micrographs displaying PV-
250 immunoreactivity (left), GABA-immunoreactivity (middle) and merge of both (right)
251 within the LHb. **(aii)** Zoom of boxed region in (ai) depicting PV-immunoreactive
252 neurons which did not co-localise with GABA. **(aiii)** Zoom of boxed region in (ai)
253 depicting a PV-immunoreactive neuron which did co-localise with GABA. **(b)**
254 Schematic illustrating location of PV-immunoreactive only, or PV / GABA co-labelled
255 neurons throughout the LHb in the rostral-caudal plane from one mouse, in which
256 every second 60 µm section was analysed. Sub-nuclear boundaries as defined by
257 Andres et al., (1999) are indicated by dashed lines. Approximate rostral-caudal
258 distances from Bregma (in mm) are indicated. **(c)** Bar graphs showing total number of
259 GABA-immunoreactive, PV-immunoreactive and GABA / PV co-localising (Co-L) LHb

260 neurons (left) and fractions of co-localising neurons as a percentage of total PV-
261 immunoreactive and of GABA-immunoreactive neurons (right; N = 3 mice).

262

263 We sought to further characterise these neurons by assessing their physiological
264 properties. We crossed PV-IRES-Cre mice with a Cre-dependent TdTomato reporter
265 line (Ai9)[40] to generate PV-IRES-Cre::Ai9 transgenic offspring (Fig. 4a) and used
266 fluorescence-assisted patch-clamp recordings to record from PV-positive LHb neurons
267 (n = 19; N = 8 mice). Consistent with our histological data, most PV-positive neurons
268 were clustered in either the medial or lateral LHb (Fig. 4b and c). When we compared
269 the whole population of PV-positive neurons to the general population of LHb neurons
270 recorded in wild-type C57/BL6 mice (n = 28 from 5 mice), we observed PV-positive
271 neurons to have a slightly lower mean input resistance (366.2 ± 39.1 vs 544.0 ± 53.3;
272 $p$ = 0.015; two-tailed unpaired t-test) and similar resting membrane potential (-59.4 ±
273 2.6 vs -55.2 ± 1.4; $p$ = 0.13; two-tailed unpaired t-test; Fig. 4di). However, the PV-
274 positive neurons in the medial and lateral LHb could clearly be differentiated based on
275 their physiological profile (Fig. 4dii and e). PV-positive neurons in the medial LHb
276 frequently exhibited sub-threshold voltage oscillations (6 of 8 medial LHb neurons)
277 while their counterparts in the lateral LHb did so very rarely (1 of 11 lateral LHb
278 neurons, $p$ = 0.006; Fishers exact test; Fig. 4e). Furthermore, a second distinctive
279 population of PV-positive neurons appeared in the lateral LHb, identifiable by their
280 hyperpolarized resting membrane potential (5 of 11 lateral LHb neurons; -77.0 ± 1.3
281 vs -59.4 ± 2.6 for all 19 PV-positive neurons; $p$ = 0.001; two-tailed unpaired t-test) and
282 lack of rebound action potential discharge (Fig. 4dii and e), a hallmark phenotype of
283 LHb neurons[16,33,34].

284 We also performed morphological reconstruction of these neurons (Fig. 4f). Ten
285 neurons were sufficiently reconstructed to visualize a prolonged section of the axon.
286 In nine of these, this was an unbranching axon, possibly indicative of a projection
287 neuron (Fig. 4f). However, as the focus of this study was on local inhibitory control
288 within the LHb, we did not further test possible downstream projection targets of these
289 neurons. In the one remaining neuron, we did observe the axon to branch locally and
290 extensively, suggesting this to be a locally-targeting neuron. To study the local
291 connectivity of PV-positive LHb neurons, we also performed dual electrophysiological
292 recordings of PV-positive neurons and other non PV-expressing neurons within the
293 LHb (n = 7 connections tested) and only observed one postsynaptic IPSC from these
294 recordings, upon electrical stimulation of this neuron with a 2 ms depolarizing current
295 injection (Fig. 4g).

296 Taken together, these results indicate that PV-positive LHb neurons can be further
297 divided into multiple distinct sub-populations. While we do find that a small proportion
298 of these are GABAergic, the majority are non-GABAergic neurons which we assume
299 to be projection neurons. Furthermore, these non-GABAergic neurons can be
300 classified into distinct sub-populations based on physiological profile and location
301 within the LHb.

302

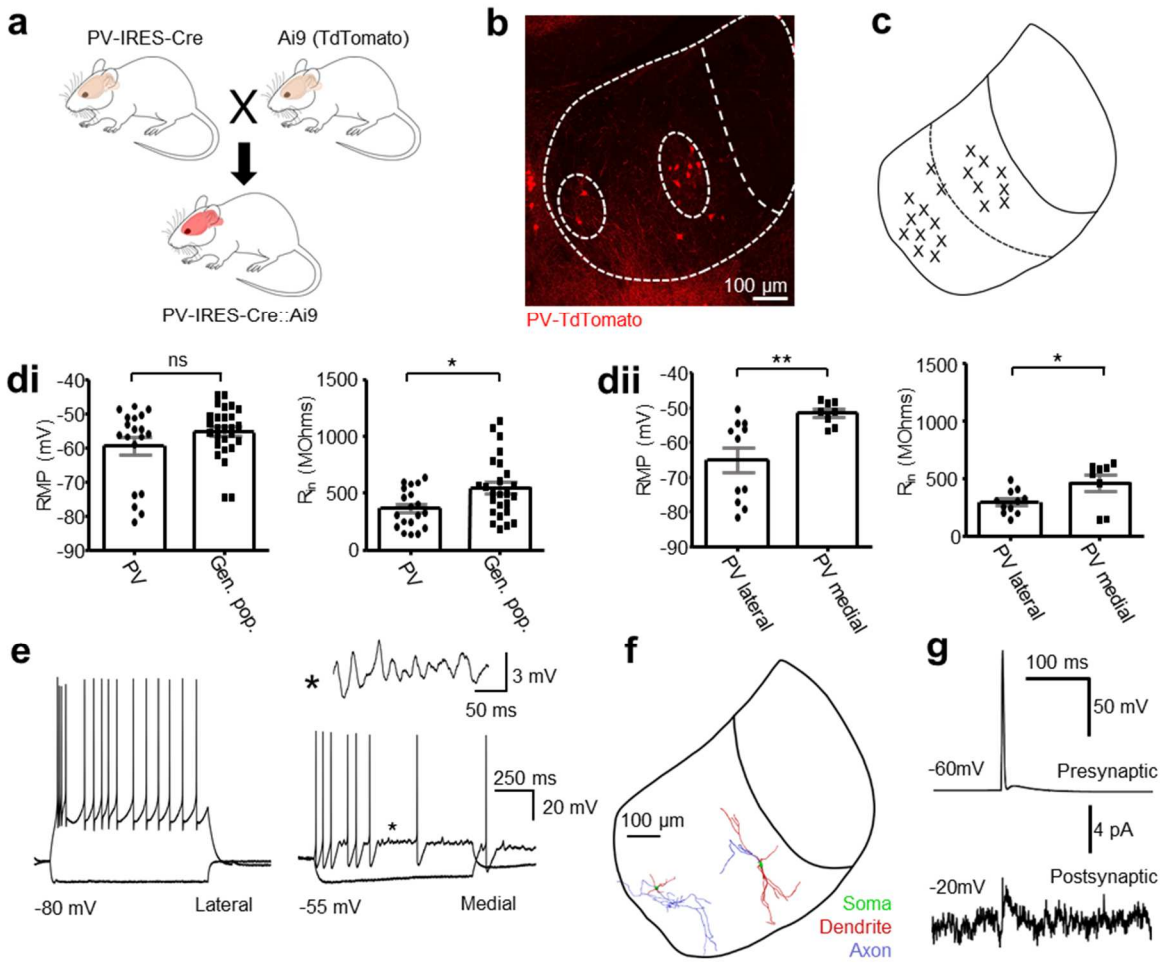


**Figure 4: PV-positive LHb neurons comprise multiple physiologically diverse populations. (a)** Schematic illustrating breeding scheme for generating PV-IRES-Cre::Ai9 mice. **(b)** Confocal micrograph depicting localization of PV-positive neurons within the LHb. The central and oval sub-nucleus approximate boundaries are indicated by dashed white lines. **(c)** Schematic illustrating location of patched neurons throughout the habenular complex. In this case, all neurons recorded have been compressed onto one schematic to allow clear visualization of neurons recorded in the lateral vs medial LHb. **(di)** Comparison of passive properties of PV-positive LHb neurons (n = 19; N = 8 mice) and from the general population of LHb neurons recorded in C57 mice (n = 28; N = 5 mice), and **(dii)** comparison of the same properties between PV positive neurons in the lateral LHb (n = 11) and medial LHb (n = 8). Data are mean

315 ± SEM. **(e)** Example traces from PV-positive neurons in response to current injection.
316 Left: traces from a neuron in the lateral LHb. Right: traces from a neuron in the medial
317 LHb Asterisk indicates a section from the recording displaying characteristic sub-
318 threshold voltage oscillations. Current steps: -50 pA and 50 pA; 1 s duration. **(f)**
319 Example reconstructions from two PV-positive neurons. Left: a neuron with an
320 extensively-branching axon (observed in 1 of 10 reconstructions). Right: a
321 representative reconstruction of neuron which displays an unbranching axon
322 (observed in 9 of 10 reconstructions). **(g)** Example traces from a presynaptic PV-
323 positive neuron electrically stimulated to fire an action potential (top; note this is the
324 same neuron as is reconstructed in E; right), and the corresponding IPSC in the
325 simultaneously recorded postsynaptic neuron.

326

327 **Input to the lateral habenula from PV-positive neurons is both excitatory and**
328 **inhibitory**

329 Previous studies have reported excitatory PV-positive neurons which project to the
330 LHb[21,41]. Considering this information, and also having observed a population of
331 inhibitory PV-positive LHb neurons (Fig. 3), we next asked whether PV-positive
332 neurons mediate primarily excitatory or inhibitory transmission within the LHb. We
333 crossed PV-IRES-Cre mice with Ai32[35] reporter mice to generate offspring where both
334 ChR2 and eYFP are expressed under the control of the PV promoter (Fig 5a). In these
335 transgenic mice, eYFP is expressed uniformly across the whole neuron. Thus,
336 sectioning and imaging of PV-IRES-Cre::Ai32 brains (N = 2) allowed us to visualize
337 both PV-positive somata and fibres within the LHb (Figs. 5b and S5). As with the
338 staining data (Fig. 3), and data from the PV-IRES-Cre::Ai9 line (Fig. 4a), PV-positive

339 somata were mostly confined to two clusters in either the medial or lateral LHb (Figs.
340 5b and S5). These clusters also appeared densely enriched with fibres (Figs. 5b and
341 S5), and appeared to roughly correlate to the previously described central sub-nucleus
342 of the medial LHb, or oval sub-nucleus of the lateral LHb[42]. While this dense
343 enrichment of fibres could be processes from local PV-positive neurons, we
344 speculated that they may also be from upstream PV-positive projection neurons, as
345 these are known to specifically target the oval sub-nucleus of the LHb[21].

346 We made acute slices from these offspring, and optogenetically stimulated PV-
347 positive neurons while recording from the general population of LHb neurons in whole-
348 cell configuration (Fig. 5c, N = 19 animals). Photostimulation-induced postsynaptic
349 potentials were observed in 29 of 76 (38.2 %) neurons recorded (Fig. 5d-f). The
350 majority of these (18 of 29; 62.1 %) displayed a solely excitatory response (Fig. 5d, f
351 and g). However, solely inhibitory responses were also observed with relative
352 frequency (6 of 29 responsive cells; 20.7%) while on two occasions, we recorded
353 postsynaptic potentials consisting of both an excitatory and inhibitory component (Fig.
354 5d, f and g). Furthermore, inhibitory postsynaptic potentials (IPSPs) were comparably
355 larger than excitatory postsynaptic potentials (EPSPs) (mean 5.6 ± 1.3 vs 2.3 ± 0.6
356 mV, respectively; $p$ = 0.013; unpaired t-test; Fig. 5g). In three of these neurons, the
357 induced IPSP was sufficiently large to momentarily silence spontaneous action
358 potential discharge of the recorded neuron (Fig. 5g & h) in a manner which could be
359 blocked by application of GABAzine. For comparison we also recorded from neurons
360 in L2/3 of the somatosensory cortex (data not shown). Here, photostimulation could
361 reliably induce action potential discharge in fast-spiking PV-positive neurons (data not
362 shown). We also recorded from L2/3 pyramidal neurons (n = 7). In these neurons,
363 photostimulation induced a large IPSP, which interestingly consisted of both a $GABA_A$

and a $GABA_B$-mediated component (data not shown, n = 3 neurons tested). Hence, PV expression is confined to inhibitory neurons which target local pyramidal neurons in L2/3 of the somatosensory cortex. In contrast, we report that input PV-positive neurons mediate both excitatory and inhibitory input to the LHb.

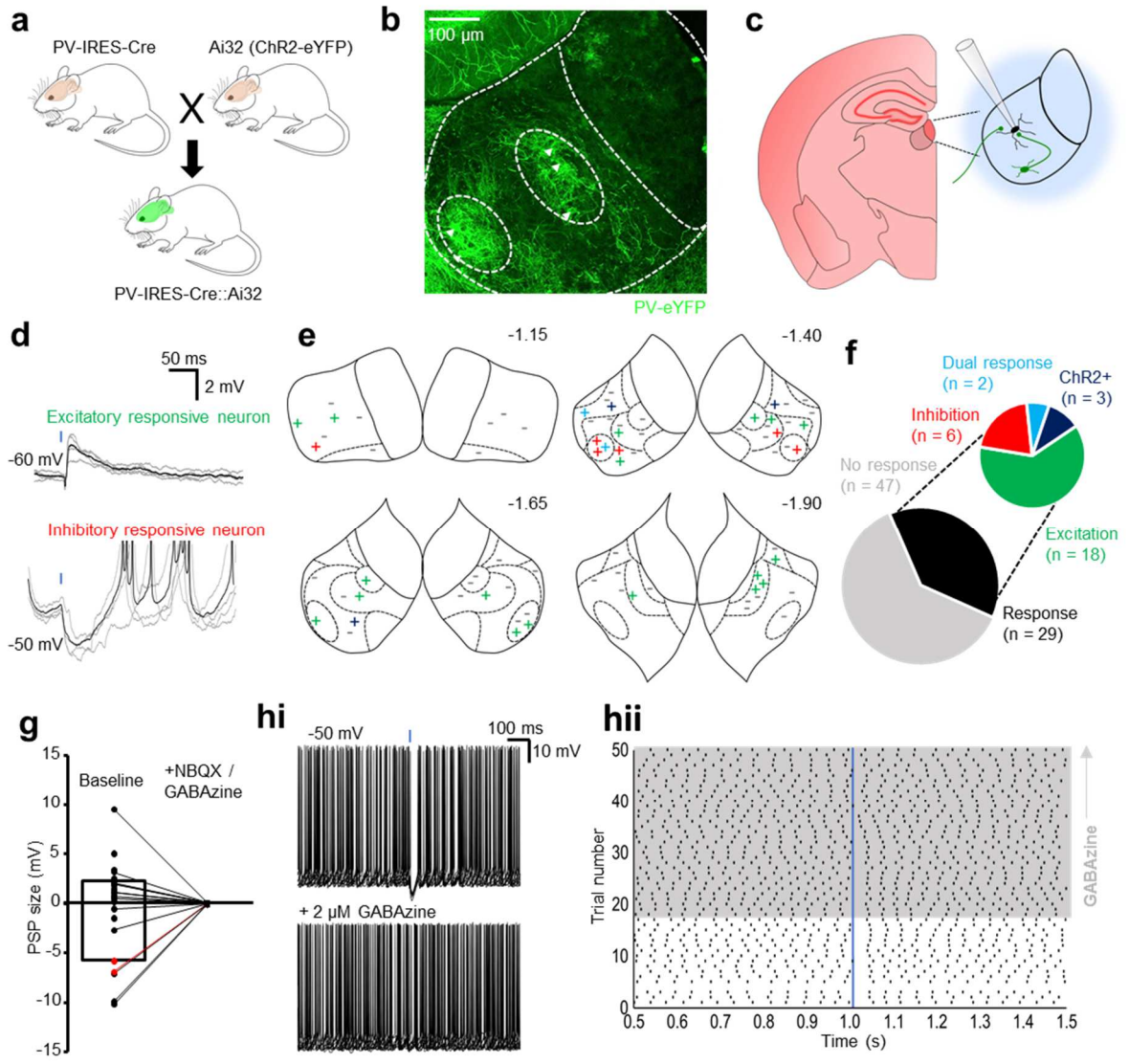


**Figure 5: PV-positive neurons mediate both excitatory and inhibitory neurotransmission within the lateral habenula. (a)** Schematic illustrating breeding scheme for generating PV-IRES-Cre::Ai32 mice. **(b)** Representative confocal

373 micrograph depicting location of both PV-positive somata and fibres within the LHb.
374 Arrowheads indicate PV-positive somata. **(c)** Schematic of recording scheme. LHb
375 neurons were patched and blue light was used to stimulate both local and long-
376 distance PV-positive neurons. **(d)** Example traces from two separate neurons in which
377 light stimulation elicited an EPSP (top) and one in which it elicited an IPSP (bottom).
378 Traces are averages of multiple traces superimposed over the traces from which the
379 average was derived. Blue square denotes 2 ms light pulse. **(e)** Schematic illustrating
380 location of patched neurons within the habenular complex, projected rostrally (top left)
381 through caudally (bottom right). Non-responsive neurons are indicated by – while
382 responsive neurons are indicated by: + EPSP only; + IPSP only; + dual response
383 consisting of both an excitatory and inhibitory component and; + ChR2-expressing
384 neuron in which an action potential not sensitive to NBQX was triggered upon
385 photostimulation. Sub-nuclear boundaries as defined by Andres et al., (1999) are
386 indicated by dashed lines. Approximate rostral-caudal distances from Bregma (in mm)
387 are indicated. **(f)** Pie-chart summarizing (d). Pie-of-pie sub-categorizes neurons based
388 on response to light-stimulation. **(g)** Before-after plot showing PSP size for neurons
389 responsive to light which exhibited EPSPs (n = 16; note 2 neurons did not display a
390 measurable EPSP at -50 mV) and IPSPs (n = 6) at -50 mV and with application of
391 either GABAzine (2 μM) or NBQX (10 μM) to abolish the PSP. Two neurons which
392 displayed both excitatory and inhibitory components are highlighted in red. One of
393 these neurons was tested pharmacologically, where both GABAzine and NBQX were
394 applied to fully abolish the PSP (red line). **(hi)** Example traces overlaid from a neuron
395 in which light-stimulation was sufficient to inhibit spontaneous action potential firing
396 (top), and which was completely blocked in the presence of GABAzine (bottom). **(hii)**

397 Raster plot of (Gi). Grey area denotes presence of GABAzine. Blue bar denotes light
398 2 ms light stimulation.

399

400 **Distinct intrinsic and extrinsic inhibitory inputs to the lateral habenula arise**
401 **from PV-positive neurons**

402 The excitatory input from PV-positive neurons to the LHb that we observed is
403 consistent with previous excitatory projections reported in the rodent entopeduncular
404 nucleus[21] and the ventral pallidum[41]. However, the inhibitory responses remain
405 unaccounted for. Referring to our histological data (Fig. 3) and dual recordings in PV-
406 IRES-Cre::Ai9 slices (Fig. 4f), we show that these GABA-immunoreactive PV neurons
407 are likely mediating local inhibition. To further test this, we intracranially injected PV-
408 IRES-Cre mice (N = 6) with a Cre-dependent AAV (Fig. 6a and methods) driving
409 expression of ChR2 and eYFP in Cre-expressing neurons into the LHb, so as to
410 express ChR2 selectively in PV-positive LHb neurons.

411 Two or more weeks following surgery, we observed robust eYFP expression within
412 the LHb (Fig. 6b and f). Recording from LHb neurons (n = 36) we occasionally
413 observed inhibitory responses upon photostimulation (n = 3), but observed no
414 excitatory responses (Fig. 6c-e). Together with our histological (Fig. 3) and
415 electrophysiological (Fig. 4f) data, these results indicate the existence of a small sub-
416 population of locally-targeting inhibitory PV-positive neuron.

417 However, while our vector clearly drove transgene expression in the LHb, we found
418 that the viral spread could occasionally not be exclusively confined to this structure,
419 likely due to the high neuronal tropism of AAV of serotype 9[43]. Thus, we observed

420 some infection in nearby thalamic neurons (Fig. 6g). In particular we noted that the
421 medial-dorsal thalamic nucleus (MDT) directly ventral to the habenular complex
422 appeared to exhibit a high number of infected neurons (Fig. 6f).

423 A recent study has identified that the lateral geniculate nucleus of the thalamus
424 projects to the LHb[15] and we therefore speculated upon another connection between
425 the MDT and the LHb. By targeting injections to the ventral MDT, we could confine
426 injections to this region without infecting the LHb (N = 6 mice, Fig. 6g and hi). Upon
427 confocal imaging, we could visualize fibres which appeared to be projecting dorsally
428 from neuronal somata located in the MDT to the LHb (Fig. 6hii). Consistently, we
429 recorded from LHb neurons (n = 47) while photostimulating MDT PV-positive neurons
430 and observed inhibitory events in seven neurons (Fig. 6i and j; note in three these
431 were only visible when the neuron was strongly depolarized). Strikingly, and consistent
432 with our observation of fibre enrichment (Fig. S5), these fibres appeared to be
433 exclusively targeting the lateral LHb; particularly the oval sub-nucleus[42] where all
434 responsive neurons were recorded (Fig. 6k). Taken together, these results provide
435 evidence for two distinct populations of inhibitory PV-positive neurons which provide
436 input to the LHb; one local, and a second population of inhibitory projection neurons
437 in the MDT.

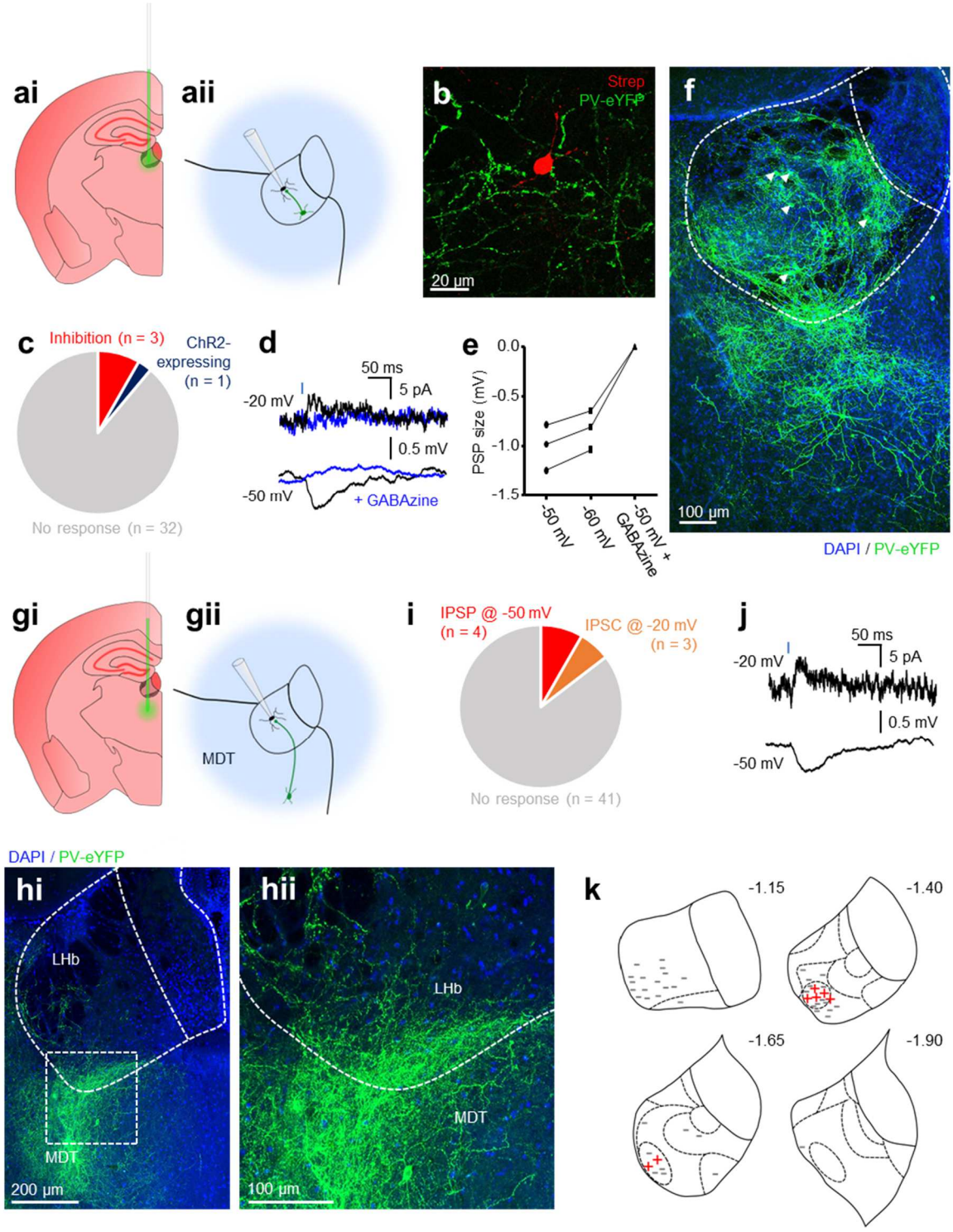


**Figure 6: Distinct inhibitory inputs to the LHb arise from local PV-positive neurons, and from neurons in the medial dorsal thalamic nucleus. (ai)** Schematic illustrating stereotaxic injection protocol into the LHb. **(aii)** Schematic illustrating electrophysiology recording protocol for LHb neurons following stereotaxic viral

injection. Transduced PV-positive neurons are photostimulated while recording from nearby LHb neurons. **(b)** Confocal micrograph depicting a neuron which displayed an IPSP upon photostimulation and surrounding fibres from PV-positive neurons. **(c)** Pie chart quantifying fraction of neurons responsive to photostimulation. **(d)** Example traces from one neuron in which an IPSP could be elicited following photostimulation in voltage clamp (top) and current clamp (bottom). Blue bar denotes 2 ms photostimulation. **(e)** Before-after plot of the IPSP amplitude from 3 different neurons at different holding potentials and after application of GABAzine (2 neurons). **(f)** Confocal micrograph depicting neurons transduced to express eYFP following viral injection. Note that while expression is clearly observed within the LHb, neurons in the dorsal thalamus are also transduced. **(gi)** and **(ii)** As for (ai and ii), but with MDT injection protocol. **(hi)** Confocal micrograph depicting eYFP expression within the MDT following stereotaxic viral injection. **(hii)** Zoom of the outlined region in (Hi). Note the presence of fibres originating from neurons in the MDT which penetrate the LHb. **(i)** and **(j)** As for (c) and (d), but with MDT injection protocol. **(k)** Schematic illustrating location of patched neurons throughout the habenular complex. All neurons responsive to photostimulation were located in the oval sub-nucleus of the lateral habenula. Sub-nuclear boundaries as defined by Andres et al., (1999) are indicated by dashed lines. Approximate rostral-caudal distances from Bregma (in mm) are indicated.

464 ## Discussion

465 In this study we sought to address the issue of inhibitory control within the LHb. We
466 implemented the use of two markers known to represent distinct sub-populations of
467 inhibitory neurons within the neocortex[24,27,28], hippocampus[25] and striatum[26]. We
468 provide evidence for two distinct sources of inhibitory input to the LHb mediated by
469 populations of PV-positive neurons. Additionally, our work serves to challenge the
470 association of these markers with inhibitory identity outside of the defined regions in
471 that both of these markers are largely associated with excitatory transmission in the
472 LHb, and that many PV-positive LHb neurons are non-GABAergic.

473 **PV neurons provide input to the LHb from a variety of sources**

474 The subject of locally-targeting inhibitory neurons within the LHb has classically been
475 a topic of debate[16,44]. In this work we show that at least two distinct populations of PV-
476 positive neurons provide inhibitory input to the LHb; one locally-targeting and one
477 located ventrally in the MDT. Strikingly, these neurons appear to selectively target
478 neurons located within the lateral LHb; particularly the oval sub-nucleus (Figs. 6d and
479 k). While the efferent targets of the LHb have long been known[45], dissecting the output
480 pathways with respect to distinct habenular sub-regions is a relatively novel idea[46].
481 Indeed it is now known that topographical organisation of LHb outputs exist and it is
482 believed that neurons in the lateral LHb specifically project to the rostromedial
483 tegmental nucleus (RMTg)[46], the primary inhibitory modulator of the VTA[47,48]. Thus it
484 is interesting to speculate whether these two distinct sources of inhibition converge
485 specifically on RMTg-projecting neurons in the lateral LHb. If this were to be the case,
486 theoretically these neurons would be well poised to reduce excitatory output to the
487 RMTg and reduce the 'reward aversion' signalling from the LHb[3,7]. Further work

488 employing *in vivo* optogenetic and chemogenetic manipulations in combination with
489 behavioural testing could serve to answer these questions.

490 In addition to these two populations of PV-positive inhibitory neurons, our results
491 also imply the existence of several physiologically diverse sub-populations of PV-
492 positive neurons within the LHb (Fig. 4), which we assume to be projection neurons.
493 These neurons possess clearly distinct physiological properties from the generic LHb
494 neuron physiology[16,33,34,] and also appear to be roughly obey sub-nuclear
495 boundaries[42]. Thus we also speculate that these neurons may have differing projection
496 targets and consequently differing functions. Further studies employing the use of Cre-
497 dependent viral tracers are necessary to delineate the circuitry that these projection
498 neurons comprise.

499 **An absence of markers for studying the role of neurogliaform cells in the LHb**

500 Selective markers for studying the role of inhibitory neurogliaform cells in cortical
501 circuits have been sparse[30] and we thus sought to validate the use of Ndnf as such a
502 marker in the somatosensory cortex[27]. Our results are consistent with other recent
503 reports[28,29] in that we find Ndnf to be mostly, but not exclusively, confined to inhibitory
504 neurons which mediate inhibitory transmission through both $GABA_A$ and $GABA_B$
505 receptors (Fig. S2). In contrast we find no such evidence in the LHb (Fig. 2).
506 Consistently, we observed no neuronal somata positive for NPY (Fig. S1). Therefore,
507 our results do not support the notion of the existence of neurogliaform cells within the
508 LHb[16,17]; or at least not those with similar molecular marker expression to those
509 described in the neocortex[27–29]. However, these previous works were carried out in rat,
510 hence we cannot exclude that this discrepancy is simply a species difference. We did
511 observe GABA-immunoreactive Ndnf-positive LHb neurons. However, these only

512 represent a small fraction of Ndnf-positive neurons (Fig. 2b). Hence, while it is
513 therefore possible that neurogliaform cells are present within the mouse LHb, we
514 conclude that neither Ndnf nor NPY can be used as a marker to study them.

515 **A need for sub-classifying LHb neurons based on physiology properties and**
516 **molecular marker expression**

517 Much invaluable information regarding the LHb has come from histological[44,42,49] and
518 transcriptomic studies[17,32,50]. These works have provided great insight into the
519 organization of the LHb neuronal circuitry with reference to particular protein and gene
520 expression patterns. However, these approaches do not permit these findings to be
521 correlated with neuronal physiology at the single cell level. Indeed, recent reports have
522 highlighted that individual LHb neurons which exhibit 'bursting' physiological
523 phenotypes are associated with depression[11,12], and thus a greater understanding of
524 LHb neuronal physiology, and how this physiology links to molecular protein
525 expression is of great value.

526 Within this work, we have approached this problem by investigating the
527 physiological properties of neurons expressing defined molecular markers. In the case
528 of PV-positive LHb neurons alone, we show that these can be sub-classified into
529 inhibitory neurons, and at least two distinct classes of non-inhibitory neurons. Thus,
530 implementing the use of further molecular markers will allow further sub-classification
531 of LHb neurons with respect to these markers and physiological properties, which can
532 also provide a platform to link novel circuitry to behavioural outcome.

533

534 **The role of inhibitory signalling within the LHb**

535 What could be the role of inhibitory signalling within the LHb? It is well established that
536 the LHb is hyperactive in MDD[6–12], and that reducing LHb hyperexcitability by altering
537 the balance of excitatory and inhibitory signalling has an antidepressant effect[7–9,20,21].
538 A striking feature of many neurons innervating the LHb is that they co-release GABA
539 and glutamate and hence much work has focussed on the role that these neurons play
540 in modulating LHb excitability[8,19–21,51]. Yet, both local[18] and projection[15,23] GABAergic
541 neurons are also known to innervate the LHb.

542 How these GABAergic neurons modulate the LHb in MDD remains to be fully
543 established. Indeed, one could speculate that if excitatory inputs to the LHb are
544 potentiated in MDD[7], then GABAergic tone may be enhanced. If this were to be the
545 case, then one may also speculate that increasing GABAergic tone should also have
546 an antidepressant effect. For this reason, we believe GABAergic innervation of the
547 LHb to be an important topic of study. Interestingly, our results seem to point to a target
548 selectivity of inhibitory PV-positive neurons at the sub-regional, possibly even single
549 cellular level (Figs. 6d and 4k). We also show that these inhibitory neurons are capable
550 of silencing the spontaneous activity of LHb neurons (Fig. 5h). Therefore, it is
551 reasonable to assume that the role played by these inhibitory neurons in modulating
552 LHb neuronal excitability is not negligible, and hence a greater understanding of this
553 inhibitory control is an exciting concept.

554 **Conclusions**

555 We have investigated the mechanisms of inhibitory control within the LHb and have
556 defined two distinct sources of inhibitory input from both locally-targeting PV-positive

557 LHb neurons, and from those in the MDT. We also report multiple physiologically
558 diverse populations of non-GABAergic PV-positive LHb neurons, and provide further
559 evidence[21,41] for excitatory input to the LHb from PV-positive projection neurons (Fig.
560 5). These results, combined with the lack of specificity of Ndnf for neurogliaform cells
561 within the LHb, also indicate that these markers represent broadly diverse populations
562 of neurons on a region-to-region basis and therefore these populations must be
563 validated in each case.

564

565 ## Materials and Methods

566 ### Animals

567 All procedures were approved by the Ethics committee of the University of Strathclyde,
568 Glasgow in accordance with the relevant UK legislation (the Animals (Scientific
569 Procedures) Act, 1986). Male and female mice from each strain were used in this work.
570 All animals were maintained on a C57BL/6 background, and kept on a 12:12 light/dark
571 cycle under standard group housing conditions with unlimited access to water and
572 normal mouse chow. New-born pups were housed with parents until weaning at P21.
573 To generate transgenic reporter-bearing offspring, transgenic mice of either the PV-
574 IRES-Cre (Jax. ID 017320)[52] or Ndnf-IRES-Cre (Jax. ID 025836)[27] driver lines were
575 crossed with either Ai32 (Jax. ID 025109)[35] or Ai9 (Jax. ID 007909)[40] reporter mice
576 driving expression of Channelrhodospin-2 (ChR2) and enhanced yellow fluorescent
577 protein (eYFP), or the enhanced red fluorescent protein variant tdTomato in a Cre-
578 dependent manner, respectively. The resulting offspring strains are hence referred to

579 as: PV-IRES-Cre::Ai32, Ndnf-IRES-Cre::Ai32, PV-IRES-Cre::Ai9, and Ndnf-IRES-
580 Cre::Ai9. NPY-hrGFP mice[53] were also used in this study.

581

582 **Stereotaxic viral injections**

583 PV-IRES-Cre mice (P31-48) were deeply anaesthetized via inhaled isoflurane (5 %
584 for induction; 1-2 % for maintenance), transferred to a stereotaxic frame (Narishige,
585 Tokyo, Japan) and were subcutaneously injected with the analgesics carprofen (5
586 mg/kg) in the nape and lidocaine (4 mg/kg) under the scalp. Intracranial injections were
587 made using a glass micropipette pulled using a PC-100 vertical puller (Narishige,
588 Tokyo, Japan). Under aseptic conditions, the skull was exposed and a small burr hole
589 was drilled above the habenula within the left hemisphere. The injection capillary was
590 then advanced, and ApAAV-EF1α-Switch:NLSmRuby2/ChR2(H134R)-EYFP41
591 HGHpA[54] (titre: 2 x $10^{13}$ vector genomes / mL) was injected into either the LHb or
592 medial dorsal thalamic nucleus (MDT) at a rate of 25 nL / min using a pressure
593 microinjector (Narishige, Tokyo, Japan). ApAAV-EF1α-
594 Switch:NLSmRuby2/ChR2(H134R)-EYFP41 HGHpA is a Cre-dependent adeno-
595 associated virus of serotype 9 which drives expression of ChR2 and eYFP in Cre-
596 expressing cells, or the red fluorescent protein variant mRuby2 in the absence of Cre.
597 Parameters for LHb-targeted injections were: coordinates (from Bregma, in mm) AP -
598 1.5, ML -0.4, depth 3; volume 50 nL; N = 6 mice. Parameters for MDT-targeted
599 injections were: AP -1.355, ML -0.75 depth 3.5; volume 200 nL; N = 2 mice or AP -
600 1.155, ML -0.45 depth 3.7; volume 200 nL; N = 4 mice. Note that for the MDT-targeted
601 injection coordinates were adjusted following data acquisition from the first round of
602 experiments. Following injection, the needle was left for 10 minutes to allow the virus

603 to diffuse before being slowly withdrawn. Animals were allowed to recover from
604 anaesthesia on a heat pad. Following completion of surgery, animals were given at
605 least two weeks to allow expression of the virus before acute slice preparation for
606 electrophysiology. Upon completion of electrophysiology, viral spread was assessed
607 by imaging on a Leica SP5 or SP8 confocal microscope.

608

609 **Acute brain slice preparation**

610 C57 BL/6 (N = 5; P21-28), PV-IRES-Cre::Ai32 (N = 19; P23-40), PV-IRES-Cre::Ai9 (N
611 = 8; P23-33), Ndnf-IRES-Cre::Ai32 (N = 6; P21-28), Ndnf-IRES-Cre::Ai9 (N = 5; P21-
612 36) or surgically injected PV-IRES-Cre mice (described above) were humanely
613 euthanized by cervical dislocation and immediately decapitated, and brains were
614 rapidly removed and transferred to ice-cold oxygenated (95% $O_2$; 5% $CO_2$) sucrose-
615 based artificial cerebro-spinal fluid (ACSF) solution containing (in mM): sucrose 50,
616 NaCl 87, $NaHCO_3$ 25, KCl 3, $NaH_2PO_4$ 1.25, $CaCl_2$ 0.5, $MgCl_2$ 3, sodium pyruvate 3
617 and glucose 10. Brains sections containing the habenula were then cut in the coronal
618 plane at 250-300 µm on a Leica VT1200S vibratome (Leica Biosystems, Newcastle-
619 upon-Tyne, UK). In order to ensure slices contained the habenula, the hippocampus
620 was used as a visual guidance due to the easily identifiable structure and immediate
621 proximity to the habenula. Following sectioning, slices were incubated in oxygenated
622 sucrose-based ACSF at 35 ºC for 30 minutes, and then incubated for a further 30
623 minutes at room temperature in ACSF containing (in mM) NaCl 115, $NaHCO_3$ 25, KCl
624 3, $NaH_2PO_4$ 1.25, $CaCl_2$ 2, $MgCl_2$ 1, sodium pyruvate 3 and glucose 10. Following the
625 incubation period, slices were stored at room temperature in oxygenated ACSF.

626 **Electrophysiological recordings**

627 Individual slices were transferred to a recording chamber and continually perfused with
628 oxygenated ACSF at a flow rate of 2-3 mL / min, and visualized with a Luigs and
629 Neumann LN-Scope System (Luigs and Neumann, Ratingen, Germany). The
630 habenula is easily identifiable under differential interference contrast microscopy even
631 at low magnification and hence a 4X objective was used to locate the lateral habenular
632 nucleus. A 60X objective was then used to identify suitable cells for whole-cell
633 recordings. In the case of transgenic PV-IRES-Cre::Ai9 or Ndnf-IRES-Cre::Ai9 slices,
634 TdTomato-expressing cells could be selectively visualized with an Olympus XM10
635 fluorescent camera (Olympus, Southend-on-Sea, UK) upon photostimulation with a
636 blue LED (pE-300$^{ultra}$, Cool LED, Andover, UK). Recordings were made with a
637 Multiclamp 700B Amplifier (Molecular Devices, California, USA). Glass micropipettes
638 were filled with a solution containing (in mM) potassium gluconate 125, HEPES 10,
639 KCl 6, EGTA 0.2, $MgCl_2$ 2, Na-ATP 2, Na-GTP 0.5, sodium phosphocreatine 5, and
640 with 0.2 % biocytin. pH was adjusted to 7.2 with KOH. For spontaneous current
641 measurement experiments, a reduced chloride intracellular solution was used
642 consisting of (in mM) potassium gluconate 140, potassium chloride 2, EGTA 0.2,
643 Hepes 10, NaATP 2, NaGTP 0.5 and sodium phosphocreatine 5.

644 Once in whole-cell patch mode, the intrinsic properties of LHb neurons were
645 assessed in current-clamp configuration using a stepping protocol consisting of 1 s
646 long injections of increasing current (range: -250-250 pA; step size: 10-50 pA for LHb
647 neurons and -500-1000 pA; step size 100 pA for cortical neurons). Action potential
648 firing pattern was assessed in response to depolarizing current injection, while
649 hyperpolarizing current injection allowed the characterisation of rebound action

650 potential firing of neurons. Resting membrane potential (RMP) was assessed by
651 recording the spontaneous activity of each neuron with no current injection for at least
652 30 seconds, while membrane input resistance was monitored by injecting a small
653 hyperpolarizing pulse (100 ms; -10 to -100 pA) and measuring the voltage change.
654 Spontaneous currents were observed in voltage clamp at a holding potential of -60
655 mV. Series resistance was monitored throughout. All neuronal voltage and current
656 signals were low pass-filtered at 10 kHz and acquired at 25 kHz using an ITC-18
657 digitizer interface (HEKA, Pfalz, Germany). The data acquisition software used was
658 Axograph X.

659

660 **Multi-cell recordings**

661 To assess local connectivity between PV-positive LHb neurons and other LHb
662 neurons, whole-cell patch configuration was achieved in two neurons simultaneously
663 as described above and potential presynaptic neurons were held at -60 mV in current
664 clamp configuration while potential postsynaptic neurons were held in voltage clamp
665 and depolarized to -20 mV. Characterisation of synaptic connections between
666 simultaneously patched lateral habenular neurons was achieved by repeatedly
667 stimulating one neuron at with a 2 ms depolarizing current injections sufficient to
668 reliably generate a single action potential per pulse individually, or as a train of eight
669 10-20 Hz pulses, and measuring current change where a connection was identified in
670 the postsynaptic neuron.

671

672 **Optogenetic experiments and pharmacology**

673 For optogenetic experiments, acute brain slices were prepared from transgenic PV-
674 IRES-Cre::Ai32 and Ndnf-IRES-Cre::Ai32 offspring as above in darkness. Whole-cell
675 patch configuration was achieved and neuronal recordings were obtained at varying
676 holding potentials as slices were illuminated with a blue LED pulse (a single pulse of
677 2 to 200 ms, or a train of 2 ms pulses at 10 to 100 Hz, power 11.5 mW) to elicit
678 postsynaptic events. Where required, SR-95531 (2 μM; henceforth referred to as
679 GABAzine), NBQX (10 μM) or CGP-52432 (10 μM) (all from Tocris, Bristol, UK) were
680 washed into the perfusion bath via the perfusion pump.

681

682 **Immunohistochemistry and neuronal recovery**

683 Following electrophysiological recordings, slices containing neurons which had been
684 patched and filled with biocytin were processed as previously described[39]. Briefly,
685 slices were fixed overnight in 4% paraformaldehyde (PFA) dissolved in 0.1 M sodium-
686 based phosphate buffered saline (PBS). After fixation, slices were washed 3 x 5
687 minutes in 0.1 M PBS, and then incubated for 1 hour in a blocking solution consisting
688 of 5% normal goat serum (NGS) and 1% Triton X-100. Slices were then allowed to
689 incubate on a shaker at room temperature overnight in a primary antibody mixture
690 containing 2.5% NGS and 1% Triton in PBS along with the required primary
691 antibodies. Primary antibodies and dilutions used in this study were: mouse anti-PV
692 (1/4000; Swant, Marly, Switzerland) and rabbit anti-GABA (1/200; Sigma-Aldrich,
693 Dorset, UK). Upon completion of the primary incubation step, slices were washed 2 x
694 5 minutes in 0.1 M PBS and incubated for 2-3 hours in a secondary antibody cocktail

containing the relevant secondary antibodies along with streptavidin (conjugated to Alex Fluor 488 or 647; 1/500 dilution; Life Technologies, Paisley, UK), in order to recover neurons which had been patched and filled with biocytin. The secondary antibodies used in this study were: donkey anti-mouse conjugated to Alexa Fluor 488 (1/500 dilution; Life Technologies, Paisley, UK), goat anti-rabbit conjugated to Alexa Fluor 555, 633 or 647 (1/500 dilution; Life Technologies, Paisley, UK) and supplemented with 1% Triton in PBS. Fluorophores excitable at differing wavelengths were implicated depending on whether the slice expressed YFP (Ai32 animals) or TdTomato (Ai9 animals) to minimize crosstalk. Where only neuronal recovery was required, slices were blocked as above and incubated in a solution containing streptavidin supplemented with 1% Triton in PBS. After secondary antibody incubation, slices were washed for 3 x 5 minutes in 0.1 M PBS and mounted on glass slides using Vectashield medium (containing DAPI as required, Vector Labs, Peterborough, UK) and cover-slipped.

**Intracardial perfusion and serial sectioning**

To prepare tissue for serial sectioning, PV-IRES-Cre::Ai32 (N = 2; P31-35), Ndnf-IRES-Cre::Ai32 (N = 2; P25), Ndnf-IRES-Cre::Ai9 (N = 2; P21), NPY-hrGFP (N = 2; P23) or C57 BL/6 (N = 3; P21-22) mice were terminally anaesthetized by subcutaneous injection with an overdose cocktail of 50% lidocaine and 50% euthatal. Once anaesthetized sufficiently to be non-responsive to noxious tail and toe pinch stimuli, mice were perfused through the left ventricle with 0.1 M PBS followed by perfusion with 4% PFA dissolved in PBS. Brains were then removed and fixed

718 overnight in 4% PFA in PBS, after which they were cryoprotected in a solution
719 containing 30% (w/v) sucrose in PBS for storage until required for serial sectioning.

720 For these experiments, brains were embedded in OCT compound (VWR,
721 Leicestershire, UK) and sectioned on a Leica SM2010 R microtome (Leica
722 Biosystems, Newcastle-upon-Tyne, UK) at 60-80 µm. Upon completion of sectioning,
723 slices were washed 3 x 5 min in 0.1 M PBS. Where further staining was required, this
724 was carried out as above (see immunohistochemistry and neuronal recovery),
725 however, 0.3% Triton X-100 was used in place of 1% and slices were incubated
726 overnight in primary antibody cocktails to minimize tissue damage. Slices were then
727 mounted using Vectashield medium (Vector Labs, Peterborough, UK) and cover-
728 slipped.

729

730 **Confocal Microscopy and neuronal reconstructions**

731 Mounted sections were scanned on either a Leica SP5 or SP8 confocal microscope,
732 imaging z-stacks of each slice at 2-4 µm steps. Confocal laser excitation wavelengths
733 (in nm) were 405, 488, 514, 552 and 503. Objectives used were 10X (dry), 20X (oil
734 immersion), 40X (oil immersion) and 63X (oil immersion) for Leica SP5, or 10X (dry),
735 20X (dry) and 63X (oil immersion) for SP8. A zoom of up to 2X was applied as required
736 to occasionally visualize soma in enhanced detail. Sections were scanned to ensure
737 that all visible streptavidin-stained cells and their neurites were included in the z-stack.
738 3D reconstructions of neurons were carried out using NeuTube 3D reconstruction
739 software[55].

740

741 **Data analysis**

742 Analysis of electrophysiological recordings was carried out using Axograph X. Passive
743 intrinsic properties were calculated as described above, while active intrinsic
744 properties (action potential initial frequency, amplitude, rise-time and half-width) were
745 calculated by subtracting the baseline and then using the event detection feature to
746 analysis the first action potential elicited in response to a 50 pA depolarizing pulse.
747 Neuronal spontaneous activity was classified as either bursting (a clearly distinctive
748 behaviour[16]), tonic or silent (where spontaneous action potential frequency was < 1
749 Hz). For optogenetically evoked events, peak size was measured at various holding
750 potentials. For spontaneous current measurements, representative example traces of
751 postsynaptic currents were first generated and currents were detected and measured
752 using the event detection feature.

753 Image analysis was carried out using ImageJ. Confocal z-stacks were compressed
754 into a single image and brightness and contrast were adjusted to enhance cellular
755 visualization. Total numbers of cells (using DAPI as a proxy for neuronal identity) and
756 immunoreactive neurons were counted using the cell-counter plugin. For these
757 experiments, serial sections from the whole brain were imaged and analysed from one
758 animal for each strain, and for remaining animals every second or third section was
759 imaged and analysed to allow quantification of markers with fair representation of the
760 habenular sub-nuclei. Images were then transferred to PowerPoint (Microsoft), where
761 cells of interest were marked.

762 Graphs were generated and statistical analysis was performed using GraphPad
763 Prism 5 (California, USA). Statistical tests used were either two-tailed unpaired t-test,
764 or Fishers' exact test. Once graphs were generated, they transferred to PowerPoint

765 2013 for formatting and assembly into figures. Statistical significance thresholds were:

766 * $p < 0.05$; ** $p < 0.01$; and *** $p < 0.001$.

767 ## References


768 1. Christoph GR, Leonzio RJ, Wilcox KS. Stimulation of the lateral habenula
769 inhibits dopamine-containing neurons in the substantia nigra and ventral
770 tegmental area of the rat. J Neurosci. 1986;6(3):613–9.

771 2. Ji H, Shepard PD. Lateral habenula stimulation inhibits rat midbrain dopamine
772 neurons through a GABA(A) receptor-mediated mechanism. J Neurosci.
773 2007;27(26):6923–30.

774 3. Matsumoto M, Hikosaka O. Lateral habenula as a source of negative reward
775 signals in dopamine neurons. Nature. 2007;447(7148):1111–5.

776 4. Wang RY, Aghajanian GK. Physiological evidence for habenula as major link
777 between forebrain and midbrain raphe. Science. 1977;197(4298):89–91.

778 5. Geisler S, Trimble M. The lateral habenula: No longer neglected. CNS Spectr.
779 2008;13(6):484–9.

780 6. Sartorius A, Kiening KL, Kirsch P, von Gall CC, Haberkorn U, Unterberg AW,
781 et al. Remission of Major Depression Under Deep Brain Stimulation of the
782 Lateral Habenula in a Therapy-Refractory Patient. Biol Psychiatry.
783 2010;67(2):9–11.

784 7. Li B, Piriz J, Mirrione M, Chung C, Proulx CD, Schulz D, et al. Synaptic
785 potentiation onto habenula neurons in the learned helplessness model of
786 depression. Nature. 2011;470(7335):535–9.

787 8. Shabel SJ, Proulx CD, Piriz J, Manilow R. Mood regulation. GABA/glutamate
788 co-release controls habenula output and is modified by antidepressant
789 treatment. Science. 2014;345(6203):1494–8.

790 9. Lecca S, Pelosi A, Tchenio A, Moutkine I, Lujan R, Hervé D, et al. Rescue of
791 GABAB and GIRK function in the lateral habenula by protein phosphatase 2A
792 inhibition ameliorates depression-like phenotypes in mice. Nat Med.
793 2016;22(3):254–61.

794 10. Tchenio A, Lecca S, Valentinova K, Mameli M. Limiting habenular hyperactivity
795 ameliorates maternal separation-driven depressive-like symptoms. Nat
796 Commun. 2017;8(1):1135.

797 11. Cui Y, Yang Y, Ni Z, Dong Y, Cai G, Foncelle A, et al. Astroglial Kir4.1 in the
798 lateral habenula drives neuronal bursts in depression. Nature.
799 2018;554(7692):323–7.

800 12. Yang Y, Cui Y, Sang K, Dong Y, Ni Z, Ma S, et al. Ketamine blocks bursting in
801 the lateral habenula to rapidly relieve depression. Nature.
802 2018;554(7692):317–22.

803 13. Winter C, Vollmayr B, Djodari-Irani A, Klein J, Sartorius A. Pharmacological
804 inhibition of the lateral habenula improves depressive-like behavior in an
805 animal model of treatment resistant depression. Behav Brain Res.
806 2011;216(1):463–5.

807 14. Schneider TM, Beynon C, Sartorius A, Unterberg AW, Kiening KL. Deep brain
808 stimulation of the lateral habenular complex in treatment-resistant depression:
809 Traps and pitfalls of trajectory choice. Neurosurgery. 2013;72:184–93.

810 15. Huang L, Xi Y, Peng Y, Yang Y, Huang X, Fu Y, et al. A Visual Circuit Related
811 to Habenula Underlies the Antidepressive Effects of Light Therapy. Neuron.
812 2019;102(1):128–42.

813 16. Weiss T, Veh RW. Morphological and electrophysiological characteristics of

814 neurons within identified subnuclei of the lateral habenula in rat brain slices.
815 Neuroscience. 2011;172:74–93.

816 17. Wagner F, Bernard R, Derst C, French L, Veh RW. Microarray analysis of
817 transcripts with elevated expressions in the rat medial or lateral habenula
818 suggest fast GABAergic excitation in the medial habenula and habenular
819 involvement in the regulation of feeding and energy balance. Brain Struct
820 Funct. 2016;221(9):4463–89.

821 18. Zhang L, Hernández VS, Swinny JD, Verma AK, Giesecke T, Emery AC, et al.
822 A GABAergic cell type in the lateral habenula links hypothalamic homeostatic
823 and midbrain motivation circuits with sex steroid signaling. Transl Psychiatry.
824 2018;8(1):50.

825 19. Root DH, Mejias-Aponte CA, Zhang S, Wang HL, Hoffman AF, Lupica CR, et
826 al. Single rodent mesohabenular axons release glutamate and GABA. Nat
827 Neurosci. 2014;17(11):1543–51.

828 20. Meye FJ, Soiza-Reilly M, Smit T, Diana MA, Schwarz MK, Mameli M. Shifted
829 pallidal co-release of GABA and glutamate in habenula drives cocaine
830 withdrawal and relapse. Nat Neurosci. 2016;19(8):1019–24.

831 21. Wallace ML, Saunders A, Huang KW, Philson AC, Goldman M, Macosko EZ,
832 et al. Genetically Distinct Parallel Pathways in the Entopeduncular Nucleus for
833 Limbic and Sensorimotor Output of the Basal Ganglia. Neuron.
834 2017;94(1):138–52.

835 22. Barker DJ, Miranda-Barrientos J, Zhang S, Root DH, Wang H-L, Liu B, et al.
836 Lateral Preoptic Control of the Lateral Habenula through Convergent
837 Glutamate and GABA Transmission. Cell Rep. 2017;21(7):1757–69.

838 23. Faget L, Zell V, Souter E, McPherson A, Ressler R, Gutierrez-reed N, et al.
839 Opponent control of behavioral reinforcement by inhibitory and excitatory
840 projections from the ventral pallidum. Nat Commun. 2018;9(1):1–14.

841 24. Tremblay R, Lee S, Rudy B. GABAergic Interneurons in the Neocortex: From
842 Cellular Properties to Circuits. Neuron. 2016;91(2):260–92.

843 25. Klausberger T, Somogyi P. Neuronal diversity and temporal dynamics: the
844 unity of hippocampal circuit operations. Science. 2008;321(5885):53–7.

845 26. Tepper JM, Tecuapetla F, Koós T, Ibáñez-Sandoval O. Heterogeneity and
846 Diversity of Striatal GABAergic Interneurons. Front Neuroanat. 2011;4(150).

847 27. Tasic B, Menon V, Nguyen TNT, Kim TTK, Jarsky T, Yao Z, et al. Adult mouse
848 cortical cell taxonomy revealed by single cell transcriptomics. Nat Neurosci.
849 2016;19(2):335–46.

850 28. Abs E, Poorthuis RB, Apelblat D, Muhammad K, Pardi MB, Enke L, et al.
851 Learning-Related Plasticity in Dendrite-Targeting Layer 1 Interneurons.
852 Neuron. 2018;100(3):684–99.

853 29. Tasic B, Yao Z, Graybuck LT, Smith KA, Nguyen TN, Bertagnolli D, et al.
854 Shared and distinct transcriptomic cell types across neocortical areas. Nature.
855 2018;563(7729):72–8.

856 30. Overstreet-Wadiche L, McBain CJ. Neurogliaform cells in cortical circuits. Nat
857 Rev Neurosci. 2015;16(8):458–68.

858 31. Choi K, Lee Y, Lee C, Hong S, Lee S, Kang SJ, et al. Optogenetic activation of
859 septal GABAergic afferents entrains neuronal firing in the medial habenula. Sci
860 Rep. 2016;6(34800).

861 32. Wagner F, French L, Veh RW. Transcriptomic-anatomic analysis of the mouse

862 habenula uncovers a high molecular heterogeneity among neurons in the
863 lateral complex, while gene expression in the medial complex largely obeys
864 subnuclear boundaries. Brain Struct Funct. 2016;221(1):39–58.

865 33. Chang S, Kim U. Ionic Mechanism of Long-Lasting Discharges of Action
866 Potentials Triggered by Membrane Hyperpolarization in the Medial Lateral
867 Habenula. J Neurosci. 2004;24(9):2172–81.

868 34. Kim U, Chang SY. Dendritic morphology, local circuitry, and intrinsic
869 electrophysiology of neurons in the rat medial and lateral habenular nuclei of
870 the epithalamus. J Comp Neurol. 2005;483(2):236–50.

871 35. Madisen L, Mao T, Koch H, Zhuo JM, Berenyi A, Fujisawa S, et al. A toolbox of
872 Cre-dependent optogenetic transgenic mice for light-induced activation and
873 silencing. Nat Neurosci. 2012;15(5):793–802.

874 36. Tamás G, Lorincz A, Simon A, Szabadics J. Identified sources and targets of
875 slow inhibition in the neocortex. Science. 2003;299(5614):1902–5.

876 37. Price CJ, Cauli B, Kovacs ER, Kulik A, Lambolez B, Shigemoto R, et al.
877 Neurogliaform Neurons Form a Novel Inhibitory Network in the Hippocampal
878 CA1 Area. J Neurosci. 2005;25(29):6775–86.

879 38. Price CJ, Scott R, Rusakov DA, Capogna M. GABA(B) receptor modulation of
880 feedforward inhibition through hippocampal neurogliaform cells. J Neurosci.
881 2008;28(27):6974–82.

882 39. Wozny C, Williams SR. Specificity of synaptic connectivity between layer 1
883 inhibitory interneurons and layer 2/3 pyramidal neurons in the rat neocortex.
884 Cereb Cortex. 2011;21(8):1818–26.

885 40. Madisen L, Zwingman TA, Sunkin SM, Oh SW, Zariwala HA, Gu H, et al. A

886 robust and high-throughput Cre reporting and characterization system for the
887 whole mouse brain. Nat Neurosci. 2010;13(1):133–40.

888 41. Knowland D, Lilascharoen V, Pham Pacia C, Shin S, Hou-Jen Wang E, Kook
889 Lim B, et al. Distinct Ventral Pallidal Neural Populations Mediate Separate
890 Symptoms of Depression. Cell. 2017;170(2):284–97.

891 42. Andres KH, Von Düring M, Veh RW. Subnuclear organization of the rat
892 habenular complexes. J Comp Neurol. 1999;407(1):130–50.

893 43. Aschauer DF, Kreuz S, Rumpel S. Analysis of Transduction Efficiency,
894 Tropism and Axonal Transport of AAV Serotypes 1, 2, 5, 6, 8 and 9 in the
895 Mouse Brain. PLoS One. 2013;8(9).

896 44. Brinschwitz K, Dittgen A, Madai VI, Lommel R, Geisler S, Veh RW.
897 Glutamatergic axons from the lateral habenula mainly terminate on GABAergic
898 neurons of the ventral midbrain. Neuroscience. 2010;168(2):463–76.

899 45. Herkenham M, Nauta WJH. Efferent connections of the habenular nuclei in the
900 rat. J Comp Neurol. 1979;187(1):19–47.

901 46. Quina LA, Tempest L, Ng L, Harris JA, Ferguson S, Jhou TC, et al. Efferent
902 pathways of the mouse lateral habenula. J Comp Neurol. 2015;523(1):32–60.

903 47. Jhou TC, Fields HL, Baxter MG, Saper CB, Holland PC. The Rostromedial
904 Tegmental Nucleus (RMTg), a major GABAergic afferent to midbrain
905 dopamine neurons, encodes aversive stimuli and inhibits motor responses.
906 Neuron. 2009;61(5):786–800.

907 48. Jhou TC, Geisler S, Marinelli M, Degarmo BA, Zahm DS. The mesopontine
908 rostromedial tegmental nucleus: A structure targeted by the lateral habenula
909 that projects to the ventral tegmental area of Tsai and substantia nigra

910 compacta. J Comp Neurol. 2009;513(6):566–96.

911 49. Geisler S, Andres KH, Veh RW. Morphologic and cytochemical criteria for the
912 identification and delineation of individual subnuclei within the lateral habenular
913 complex of the rat. J Comp Neurol. 2003;458(1):78–97.

914 50. Aizawa H, Kobayashi M, Tanaka S, Fukai T, Okamoto H. Molecular
915 characterization of the subnuclei in rat habenula. J Comp Neurol.
916 2012;520(18):4051–66.

917 51. Lazaridis I, Tzortzi O, Weglage M, Märtin A, Xuan Y, Parent M, et al. A
918 hypothalamus-habenula circuit controls aversion. Mol Psychiatry. 2019 [Epub
919 ahead of print]

920 52. Hippenmeyer S, Vrieseling E, Sigrist M, Portmann T, Laengle C, Ladle DR, et
921 al. A developmental switch in the response of DRG neurons to ETS
922 transcription factor signaling. PLoS Biol. 2005;3(5):0878–90.

923 53. van den Pol AN, Yao Y, Fu L-Y, Foo K, Huang H, Coppari R, et al.
924 Neuromedin B and Gastrin-Releasing Peptide Excite Arcuate Nucleus
925 Neuropeptide Y Neurons in a Novel Transgenic Mouse Expressing Strong
926 Renilla Green Fluorescent Protein in NPY Neurons. J Neurosci.
927 2009;29(14):4622–39.

928 54. Wozny C, Beed P, Nitzan N, Pössnecker Y, Rost BR, Schmitz D. VGLUT2
929 functions as a differential marker for hippocampal output neurons. Front Cell
930 Neurosci. 2018;12(337).

931 55. Feng L, Zhao T, Kim J. neuTube 1.0: A New Design for Efficient Neuron
932 Reconstruction Software Based on the SWC Format. eNeuro. 2015;2(1).

933

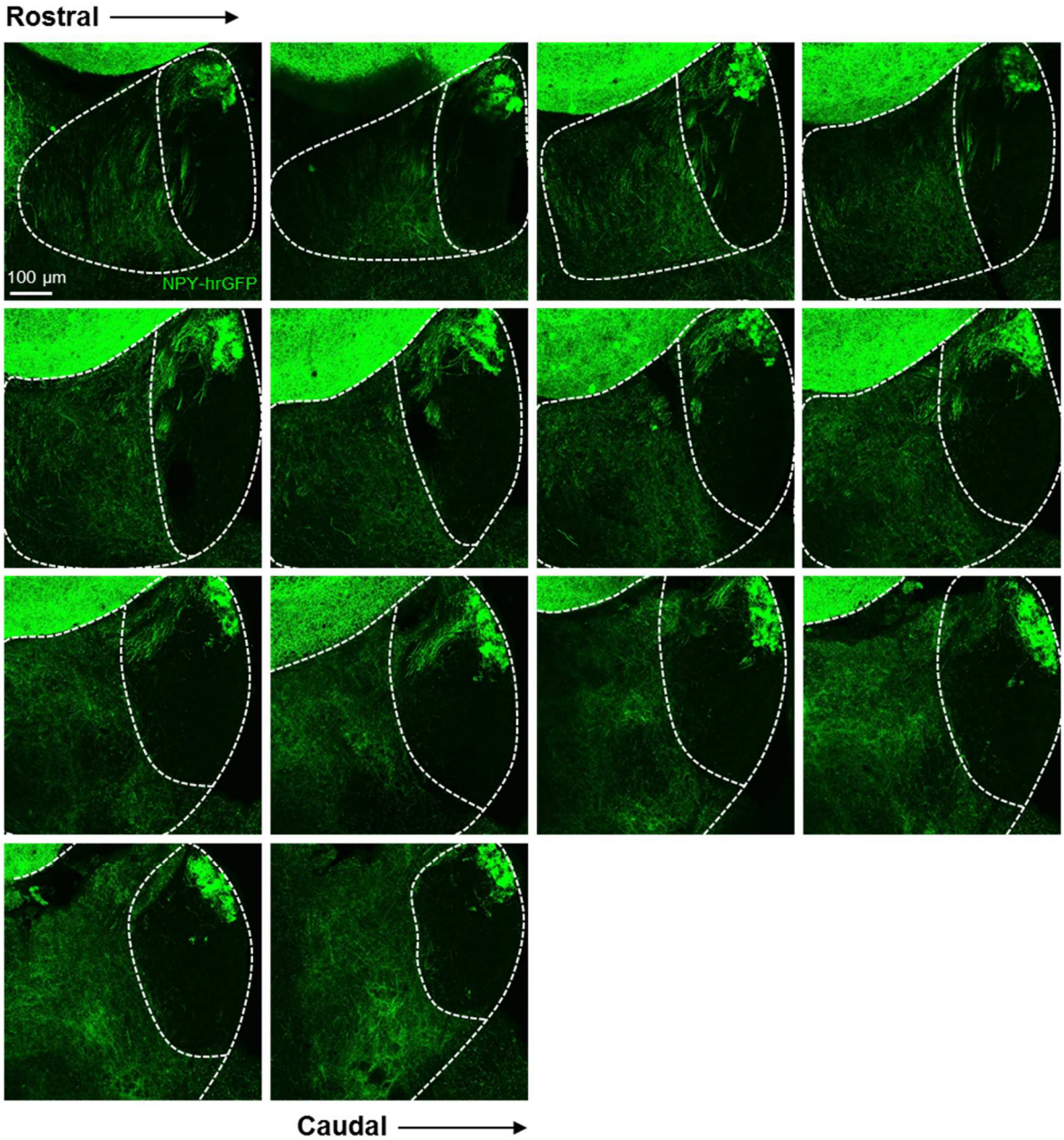


934

935 **Supplementary Figure 1: Absence of NPY-positive neuronal somata within in the**
936 **LHb.** Confocal micrographs of habenular sections from NPY-hrGFP mice (N = 2)
937 depicting NPY-expression throughout the LHb in the rostral-caudal plane. Images are
938 maximum intensity projections of 50 µm tissue. Note that no NPY-positive somata are
939 located within the LHb.

940

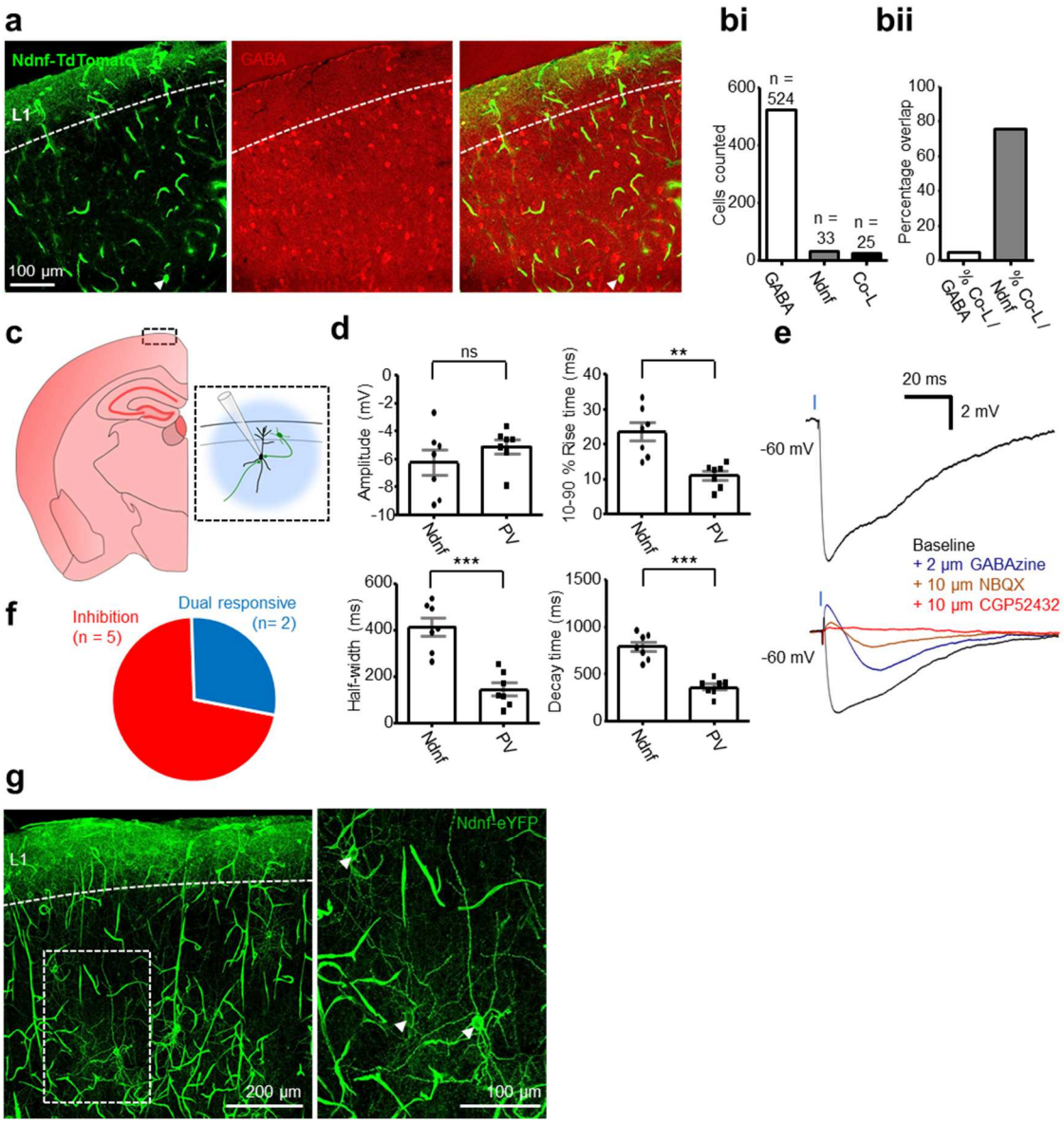


**Supplementary Figure 2: Ndnf is expressed selectively but not exclusively by L1 neurons in the somatosensory cortex. (a)** Confocal micrograph from Ndnf-IRES-Cre::Ai9 slices depicting Ndnf-positive neurons in L1 of the somatosensory cortex, but also an Ndnf-positive neuron in the deeper somatosensory cortex which was not immunoreactive for GABA. **(bi)** Bar chart quantifying total number of GABA-immunoreactive, and Ndnf-positive neurons counted and the number which co-expressed both (N = 2 mice). **(bii)** Fraction of neurons expressing both markers as a percentage of GABA-immunoreactive neurons, and as a percentage of Ndnf-positive

951 neurons. **(c)** Schematic of recording scheme. L2/3 pyramidal neurons were patched
952 and blue light was used to stimulate both local and long-distance Ndnf-positive
953 neurons. **(d)** Scatter plots comparing amplitude (-6.3 ± 0.9 mV vs -5.1 ± 0.5 mV; $p$ =
954 0.29; two-tailed unpaired t-test) and kinetics (rise time 23.5 ± 2.7 ms vs 11.1 ± 1.3 ms;
955 $p$ = 0.001; half-width 414.6 ± 39.1 ms vs 146.0 ± 27.6 ms; $p$ = 0.0001; decay 787.4 ±
956 51.9 ms vs 361.3 ± 32.8 ms; $p$ < 0.0001; two-tailed unpaired t-test) of photostimulation-
957 induced IPSPs in Ndnf-IRES-Cre::Ai32 slices vs PV-IRES-Cre::Ai32 slices. **(e)**
958 Example traces from a neuron displaying an IPSP in response to photostimulation
959 (top) and from one neuron in which an NBQX-sensitive EPSP was unmasked upon
960 application of GABAzine (bottom). **(f)** Pie chart quantifying nature of postsynaptic
961 potentials elicited in response to photostimulation. n = 7 neurons. **(gi)** Confocal
962 micrograph depicting localization of Ndnf-positive neurons in the somatosensory
963 cortex. **(gii)** Zoom-in of the same image in (gi) showing Ndnf-positive neurons not
964 located within neocortical L1 (arrowheads).

965

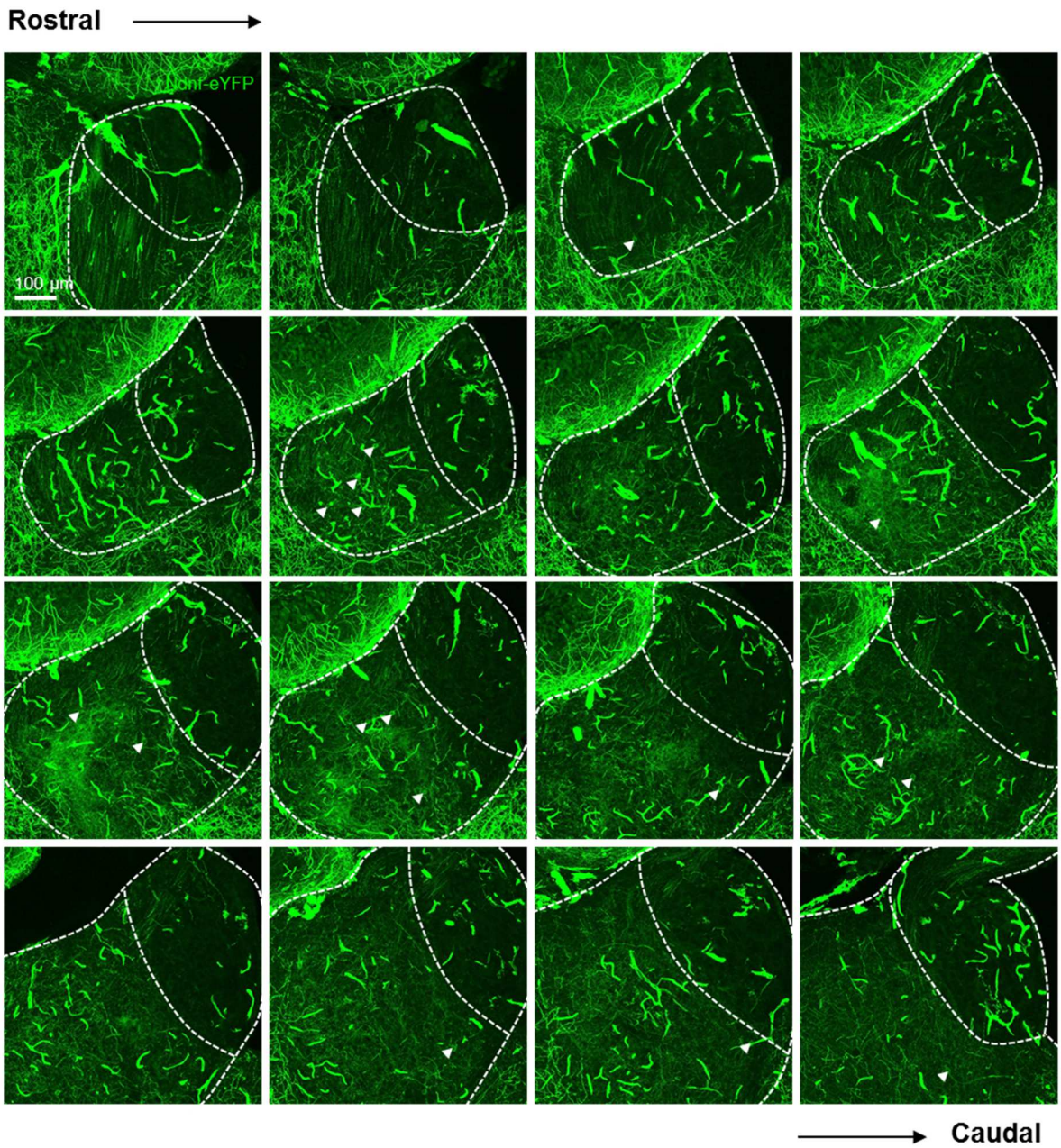


966

967 **Supplementary Figure 3**: **Localization of Ndnf-positive neuronal somata and**
968 **processes throughout the LHb.** Confocal micrographs of habenular sections from
969 Ndnf-IRES-Cre::Ai32 mice (N = 2) depicting Ndnf-expression throughout the LHb in
970 the rostral-caudal plane. Images are maximum intensity projections of the most
971 superficial 30 µm of tissue from 60 µm slices. Arrowheads indicate Ndnf-positive
972 neurons.

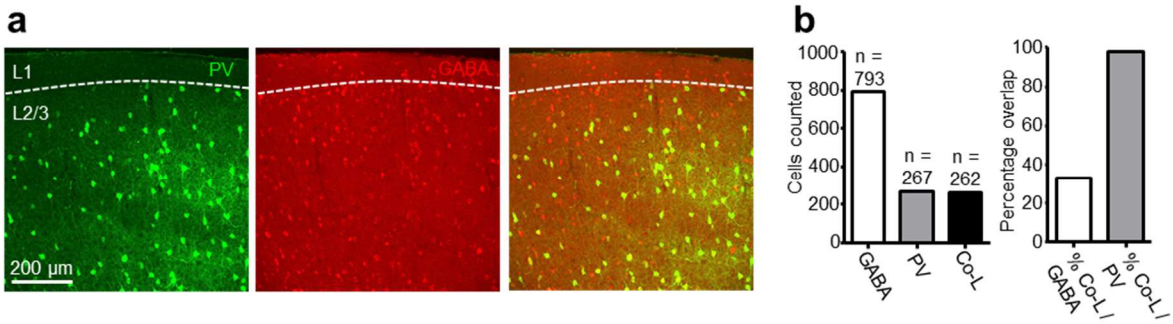


**Supplementary Figure 4: PV-immunoreactive neurons within the somatosensory cortex. (a)** Representative confocal micrographs displaying PV-immunoreactivity (left), GABA-immunoreactivity (middle) and merge of both (right) within the somatosensory cortex. (**b**) Bar graphs showing total number of GABA-immunoreactive, PV-immunoreactive and GABA / PV co-localising (Co-L) cortical neurons (left) and fractions of co-localising neurons as a percentage of total PV-immunoreactive and of GABA-immunoreactive neurons (right; N = 3 mice).

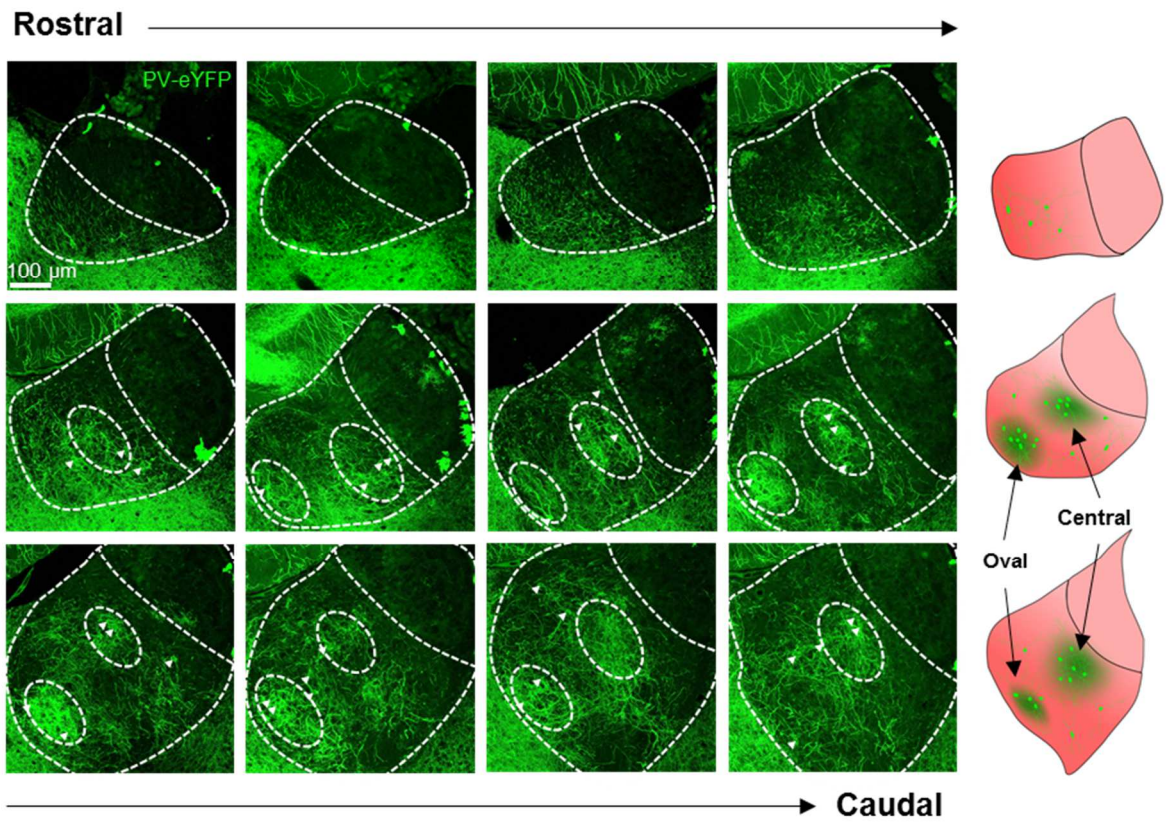


**Supplementary Figure 5: Localization of PV-positive neuronal somata and processes throughout the LHb.** Left: Confocal micrographs of 30 µm thick maximum intensity projections of habenular sections from PV-IRES-Cre::Ai32 mice (N = 2) depicting localization of PV-positive neuronal somata and neuronal processes throughout the LHb in the rostral-caudal plane. 60 µm thick spacing between images. Arrowheads indicate PV-positive neurons. Right: graphical illustrations of habenular sections indicating the oval and central lateral habenular sub-regions, where PV-expression was most prominent. Images each represent one third of the habenula in the rostral-caudal plane.